Monthly Notices of the ROYAL ASTRONOMICAL SOCIETY

MNRAS **527,** 4440–4466 (2024) https://doi.org/10.1093/mnras/stad3230
Advance Access publication 2023 October 24

Experimental atomic data of spectral lines – I. Cs, Ba, Pr, Nd, Sm, Eu, Gd, Tb, Dy, Ho, Er, Tm, Yb, Lu, Hf, Re, and Os in the 370–1000 nm interval

C. Ferrara [1,2] M. Giarrusso [2]★ and F. Leone [1,2]

[1]*Dipartimento di Fisica e Astronomia, Sezione Astrofisica, Università di Catania, Via S. Sofia 78, I-95123 Catania, Italy*
[2]*INAF – Osservatorio Astrofisico di Catania, Via S. Sofia 78, I-95123 Catania, Italy*

Accepted 2023 October 10. Received 2023 October 5; in original form 2022 October 8

ABSTRACT

Atomic data are fundamental for plasma diagnostics in laboratory and astrophysics through spectroscopy. These data are extensively present in data bases for light elements, however incomplete for high-mass atoms. This paper presents the results of systematic spectroscopy of 17 elements with high Z, expected to be produced in kilonova events generated by neutron star mergers, whose spectral lines are not yet fully identified in stellar spectra and fusion devices. Experimental data are from échelle high-resolution ($\lambda/\Delta\lambda = 60\,000$) spectroscopy of hollow cathode lamps obtained with the Catania Astrophysical Observatory Spectropolarimeter covering the 3700–10 000 Å range in a single exposure. A total of about 7700 spectral lines with energy level classification not previously listed in the NIST, Kurucz, and VALD data bases are here reported for neutral and singly ionized atomic transitions. For the spectral lines of any species, we report the measured wavelengths and their relative intensities. If possible, we also estimate the transition probabilities under the assumptions of optically thin emission and electric-dipole transitions. These are converted into oscillator strengths ready to be inserted in astrophysical data bases for spectral synthesis.

Key words: atomic data – line: identification – plasmas – methods: laboratory: atomic – techniques: spectroscopic.

1 INTRODUCTION

Knowledge of atomic data is essential for the comprehension of physical systems and applications in which atomic spectroscopy is necessary, either as a diagnostics or investigation technique from laboratory to space. An analysis of the National Institute of Standards and Technology (NIST) Atomic Spectra Database (ASD; Kramida et al. 2021) can be resumed with the following sentences on 'observed' spectral lines: (1) reasonably known for neutrals or low-ionization states up to iron-peak elements in the 200–1000 nm range, (2) poorly known for high-Z elements, and (3) almost missing for highly ionized species. Consequences are difficulties in laboratory plasma diagnostics, for example in the identification of spurious species responsible for fusion plasma cooling, or in fully exploiting spectra of astrophysical high-energy environments.

Scandium (Sc), Yttrium (Y), and Lanthanide (La; $Z = 57$–71), which are known as rare-earth elements (REEs), are characterized by common chemical and physical properties and nowadays they are very important for a lot of technological areas. From a nucleosynthesis point of view, Sc is an iron-peak element, and Y is a neutron-capture element of the first peak. The origin of REEs is still controversial in astrophysics due to their formation process that is not due to nuclear fusion in the interiors of stars (Cowan et al. 2021). A renewed interest in the atomic parameters of REEs, and in general of heavy elements, is related to the kilonova events, that is electromagnetic counterparts of neutron star merging events, which are emitters of gravitational waves. Neutron star mergers (NSMs) are supposed to be the main sites for the formation of r-process elements (Schramm & Fowler 1971). However, Kobayashi et al. (2023) revised the r-process enrichment, intending to investigate if NSMs could be the main contributor to r-process elements in the Galaxy, and they concluded these events are probably not the main origin of r-process elements. Their models adopting magnetorotational supernovae, where they use calculations by Nishimura, Takiwaki & Thielemann (2015), are the ones that reproduce best the observations. It appears that even if low-resolution spectroscopy (Smartt 2017) of the optical counterpart of GW170817 seems to support the hypothesis that NSMs are a production site of r-process elements, the ultimate proof will come from the next generation 10-m class telescopes capable of high-resolution line-by-line spectroscopy as long as atomic data of REEs are provided.

Regarding data bases of atomic transitions used in astrophysics, the major collection of spectral line data is due to Dr Robert Kurucz (Kurucz 2005), which has been used and is currently used as input for several astrophysical spectral synthesis codes (e.g. see the latest version of COSSAM; Stift & Leone 2017). The number of entries in this data base is larger for elements up to $Z \leq 30$, although most spectral line wavelengths and strengths (given in the form of $\log gf$) are theoretical and not experimentally validated. The Vienna Atomic Line Database (VALD; Ryabchikova et al. 2015) is another source of spectral line wavelengths and $\log gf$ for elements and ions of astrophysical interest. Partially extending the knowledge of spectral lines also to REEs, VALD includes both theoretical and experimental wavelengths, as well as $\log gf$. As for previous data bases, the number of atomic parameters is larger in the visible than in the ultraviolet (UV) and the near-infrared (NIR) ranges. Most of the REEs line data supplied by VALD come from the Database

★ E-mail: marina.giarrusso@inaf.it

Table 1. Elements, atomic number, supplier (GS = Green Scientific, HR = Heraeus) and part number P/N, and supply current for each lamp.

El.	Z	Suppl. + P/N	i (mA)
Cs	55	GS G810	6
Ba	56	GS G804	6
Pr	59	HR 3BNXPR-LC	15
Nd	60	GS G835	8
Sm	62	GS G847	8
Eu	63	GS G817	6
Gd	64	GS G818	8
Tb	65	HR 3BNXTB	15
Dy	66	GS G815	6
Ho	67	HR 3BNXHO	15
Er	68	HR 3BNXER	15
Tm	69	GS G859	8
Yb	70	GS G865	6
Lu	71	GS G830	8
Hf	72	HR 3QAYHF	15
Re	75	GS G843	6
Os	76	GS G838	8

on Rare Earths At Mons University (DREAM; Quinet & Palmeri 2020).

This paper presents 'large-scale' results of broad-band (3700–10 000 Å) high-resolution spectroscopy of heavy elements whose emission is observed from hollow cathode (HC) lamps (Table 1). Starting from NIST data, wavelengths, intensities, and (if possible) log gf of spectral lines are measured. We refer to NIST because entries are almost all experimental and critically evaluated before being inserted into the data base.

Section 2 regards measurements, data reduction, and analysis processes. Section 3 reports the methods used to estimate the oscillator strengths of species listed in Table 2. Section 4 resumes the results obtained (Table 3) and contains Tables (4–35) with the here-determined wavelengths, intensity, and oscillator strengths. And finally, Section 5 contains the conclusive remarks.

2 EXPERIMENTAL DATA

2.1 Spectroscopy

Spectral lines in emission have been observed from the elements listed in Table 1 and turned in plasma in HC lamps.

Data are obtained with the Catania Astrophysical Observatory Spectropolarimeter (CAOS; Leone et al. 2016), which is an échelle spectrograph covering the 3700–10 000 Å range in a single exposure, at resolution $R = \lambda/\Delta\lambda = 60\,000$ with a CCD E2V-4240 AIMO (Advanced Inverted Mode) back-illuminated 2048 × 2048, 13.5 μm pixels[2].

A sketch of the experimental set-up used for the HC lamps spectroscopy is reported in Fig. 1. In the standard CAOS set-up, the two optical fibres (blue in Fig. 1) are illuminated with the starlight in the CAOS interface that is mounted at the Cassegrain focus of the telescope. Light from calibration lamps, which are placed in a separate calibration unit, is sent to the CAOS interface through another optical fibre (orange in Fig. 1, position 1). For acquiring HC lamp spectra, the orange fibre was disconnected from the calibration unit and connected to an optical bench where REEs HC lamps were mounted (position 2). Light from each REE lamp has been focused on the orange fibre using a standard BK7 biconvex lens. In order to maximize the amount of light sent to the spectrograph, an alignment and optimization procedure has been performed for each lamp, monitoring the flux using the CAOS autoguide camera.

Lamps have been supplied using an appropriate current generator provided by Green Scientific with the currents listed in Table 1. For each element a minimum of 3 × 600 s spectra have been acquired. Such exposure time allows the extraction of the weakest lines otherwise embedded in the readout noise, avoiding largely saturated lines tearing across the whole CCD. Frames with the

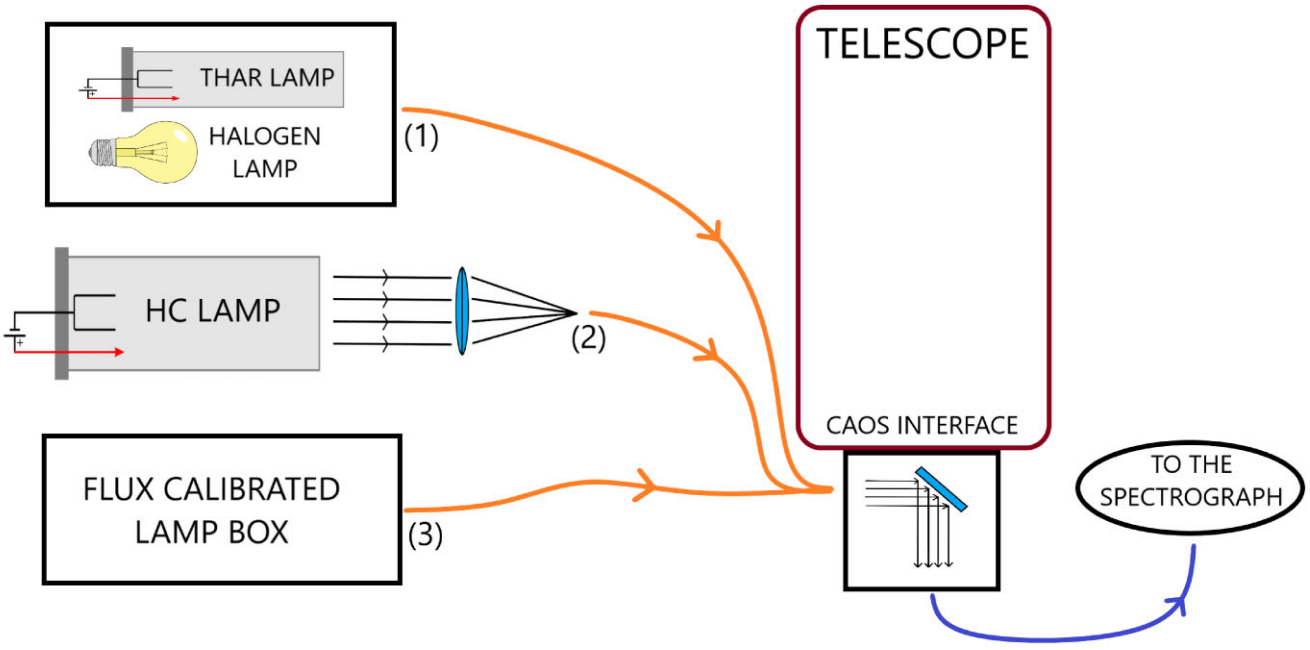

Figure 1. Schematic drawing of the experimental set-up. When the optical (orange) fibre is in position (1) collects light from the CAOS calibration unit; when it is in position (2) collects light from the HC lamp of the measured element; when it is in position (3) is connected to the flux-calibrated lamp box.

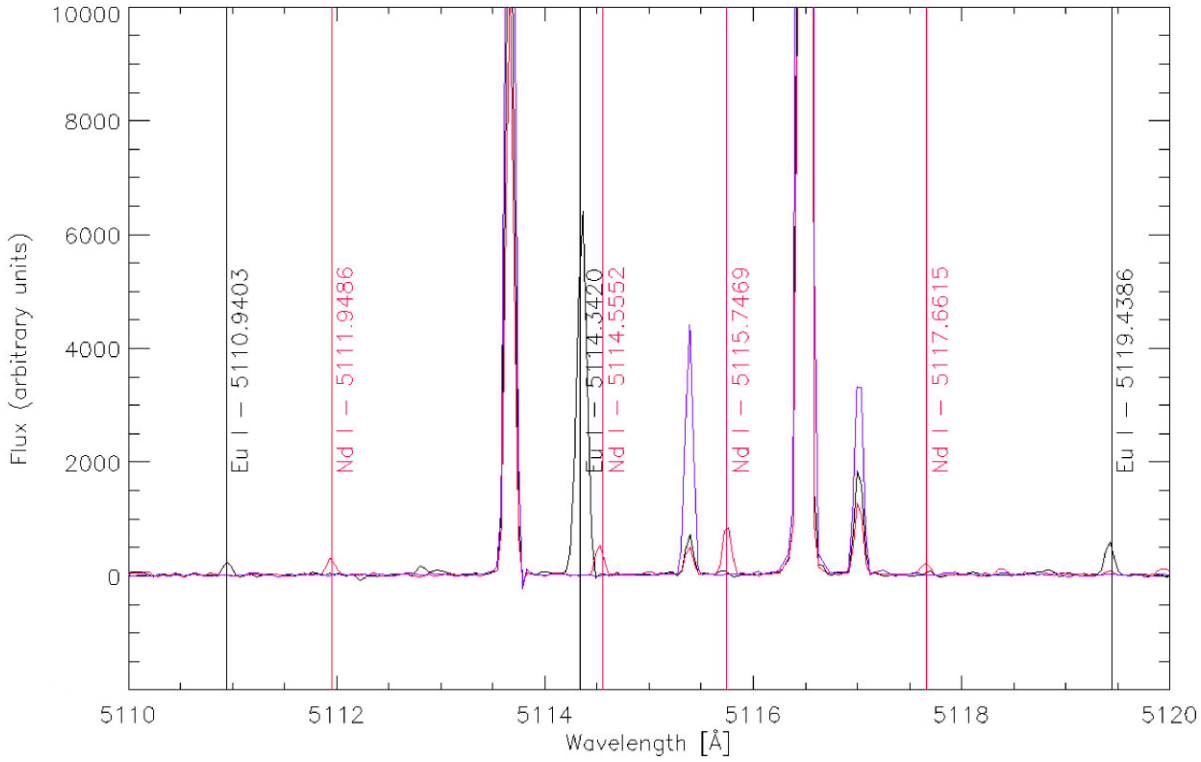

Figure 2. Eu lamp (black), Nd lamp (red), and Gd lamp (blue) emission spectra with Ritz wavelengths. As it is evident, some spectral features are common to all lamps.

same exposure time have been combined to obtain an average image eventually rejecting pixels affected by sporadic events (e.g. cosmic rays). Finally, the orange fibre has been connected to the box containing the Avantes AvaLight-DHc calibrated lamp (position 3 in Fig. 1) for the acquisition of the spectrum necessary for the relative calibration of the system, as it is explained in the following subsection.

2.2 Data reduction

Following Ripepi et al. (2015), the spectroscopic data reduction has been performed with the Image Reduction and Analysis Facility (IRAF; Tody 1986) software package.

The reduction of spectra included the subtraction of the bias frame, trimming, correcting for the flat-field and the scattered light, extraction for the orders, wavelength calibration, and relative intensity correction. The wavelength calibration is achieved using the IRAF task *ecidentify*, which performs a fitting of the line peaks of a ThAr HC lamp (supplied by the Green Scientific for astronomical use with part number P/N G858A) operated at 6 mA spectrum and assigns to each value of the line centre in pixel (and order) its wavelength value. After an interactive bootstrap, the result of such a procedure is a set of points $\lambda_i = \lambda_i(x_i, y_i)$, where y is the order number and x is the pixel number along the order. These points are then fitted with a 2D Legendre or Chebyshev polynomial, in order to derive the analytical function $\lambda = \lambda(x, y)$, which allows us to convert pixel and order values in wavelength values. For our HC lamps, the wavelength calibration is obtained from 654 spectral lines with an internal rms of 5×10^{-3} Å. Observed spectral lines are shaped by the CAOS instrumental profile, a Gaussian function consistent with the resolution $R = 60\,000$. To point out any echellogram drift and refine, lamp-by-lamp, the wavelength calibration based on ThAr lamp spectra, central wavelengths of a set of Ne I–II lines have been measured and compared with values from NIST-ASD. The comparison revealed a small ($\leq 10^{-2}$ Å) but non-negligible systematic difference between the NIST and measured wavelengths. This wavelength drift may depend on several parameters, such as CAOS room temperature and lamp-by-lamp differences in the optical fibre illumination. The measured differences are used to correct lamp spectra recalibrating those to improve the wavelength accuracy of our spectra.

To obtain HCL spectral lines with relative calibrated intensities, we have also acquired the Avantes light source spectrum ($AV_{CAOS}(\lambda)$) whose 3 per cent relative flux distribution ($AV_{Cal}(\lambda)$) is guaranteed by the manufacturer. This is made of two lamps: a deuterium lamp (2000–4000 Å) and a halogen lamp (4000–25 000 Å), which largely exceed the CAOS wavelength coverage. The relative intensity spectrum $S(\lambda)$ is given by the relation

$$S(\lambda) = S_{CAOS}(\lambda)\frac{AV_{Cal}(\lambda)}{AV_{CAOS}(\lambda)}. \quad (1)$$

The light from the Avantes lamp follows the same optical path followed by the light from the HC lamp except for the biconvex lens used to acquire REE spectra. With the BK7 transmission changing less than 2 per cent along the CAOS spectral range, the relative intensity of spectral lines could be affected by an error of the same magnitude.

2.3 Determination of spectral line wavelengths

Emission lines in HC lamp spectra are due to the element constituting the cathode and the filling gas. Here all used HC lamps are filled with neon, but the hafnium is filled with argon. The comparison of

Table 2. Electron temperature and transition probability reference for each available specie (element + ionization stage).

El.	Ion.	$T_e \pm \sigma_{T_e}$ (K)			Reference
Cs	I		–		–
	II		–		–
Ba	I	5555	±	56	NIST-ASD
	II	8490	±	123	NIST-ASD
Pr	I		–		–
	II	2938	±	52	NIST-ASD
Nd	I	3501	±	23	NIST-ASD
	II	3929	±	59	NIST-ASD
Sm	I	3128	±	8	Lawler, Fittante & Den Hartog (2013)
	II	3617	±	18	Lawler et al. (2006)
Eu	I	4553	±	30	NIST-ASD
	II	4449	±	37	NIST-ASD
Gd	I	2787	±	29	NIST-ASD
	II		–		–
Tb	I		–		–
	II		–		–
Dy	I	3776	±	18	NIST-ASD
	II	5829	±	13	NIST-ASD
Ho	I	3838	±	14	Nave (2003)
	II		–		–
Er	I	2591	±	2	NIST-ASD
	II	3704	±	34	Lawler et al. (2008)
Tm	I	4532	±	15	NIST-ASD
	II		–		–
Yb	I		–		–
	II		–		–
Lu	I	2871	±	27	NIST-ASD
	II		–		–
Hf	I	4075	±	58	NIST-ASD
	II	5742	±	75	Lawler et al. (2007)
Re	I		–		–
	II		–		–
Os	I		–		–
	II		–		–

the different lamp spectra points out the common fill gas lines and highlights the spectral lines of elements. As an example, Fig. 2 shows a 10 Å portion of the spectra of Eu, Nd, and Gd HC lamps. Both Eu and Nd spectral lines, together with common lines, are clearly visible in the spectrum. As to Hf, the comparison was against the ThAr lamp we used for the wavelength calibration.

After the identification of all common lines in all spectra, which we ascribed to neon or argon, the first step for the spectral line identification was the assumption (due to the expected relatively low temperature of HC lamps) that an element is neutral or in its first ionization state. The energy levels given in the NIST-ASD (mainly by Martin, Zalubas & Hagan 1978) were then converted in expected wavelengths for electric-dipole transitions ($\Delta J = 0, \pm 1$, parity change), the so-called Ritz wavelengths. In Fig. 2, Ritz wavelengths for Eu I (black) and Nd I (red) are marked on the spectrum. Experimental wavelengths are therefore searched in the CAOS spectra through a fit using a Gaussian profile given by

$$f(\lambda) = A_0\, \mathrm{e}^{-\frac{(\lambda - A_1)^2}{2A_2^2}} + A_3, \tag{2}$$

where A_0 represents the height of the peak, A_1 is the centroid, A_2 is the width (the 'sigma') of the Gaussian, and A_3 is the background. Initial guess for A_1 was indeed the Ritz wavelength and for A_2 the ratio $A_1/2\sqrt{2\ln 2}\,R$, where $R = \lambda/\Delta\lambda$. In practice, A coefficients are determined by minimizing the quantity

$$\chi^2 = \frac{1}{N-4}\sum_{i=1}^{N}\frac{[S_i - f(\lambda; A_0, A_1, A_2, A_3)]^2}{\sigma_i^2}. \tag{3}$$

In equation (3) N is the number ($\simeq$10) of pixels and S_i is sampling the spectral line. Errors on coefficients (σ_{A_i}) are estimated as the change in A_i to increase χ^2 by one. Intensity (in arbitrary units) of a spectral line is equal to the analytical integral of the Gaussian function (equation 2) after the subtraction of A_3:

$$I = A_0 A_2 \sqrt{2\pi}. \tag{4}$$

The uncertainty on the intensity has been calculated propagating the uncertainties on the A coefficients using standard error propagation formula with quadratic sum (Taylor 1997), which we will use also in the following sections:

$$\sigma_f = \sqrt{\left(\frac{\partial f}{\partial x}\sigma_x\right)^2 + \cdots + \left(\frac{\partial f}{\partial z}\sigma_z\right)^2}, \tag{5}$$

where $f = f(x,\ldots,z)$. By applying equation (5) to the propagation of the uncertainties for I we obtain

$$\sigma_I = \sqrt{2\pi\left(A_2^2\sigma_{A_0}^2 + A_0^2\sigma_{A_2}^2\right)}. \tag{6}$$

Therefore, the measured profile is stored as a spectral line if fitted data satisfy the following criteria:

(i) the subtraction of the fitted Gaussian profile decreases the standard deviation of the region of a factor 3 and the peak value is greater than the standard deviation of the background value of a factor 3;
(ii) the width of the line profile is consistent with that of a spectral line (to reject spikes due to bad pixels or residual cosmic rays);
(iii) the centroid A_1 discards less than the half width at half-maximum (HWHM) of the nominal CAOS resolution;
(iv) the baseline A_3 of the line does not exceed a maximum value to reject spectral lines in the region of saturated Ne lines;
(v) the intensity does not exceed a maximum value determined by the saturation value of the detector.

The result of such analysis and selection process is a list of measured quantities (wavelength and relative intensity). A detailed explanation of tables is given in Section 4. The next section explains the process that allowed, for a subset of the analysed species, an estimate of the line strengths.

3 ESTIMATE OF TRANSITION PROBABILITIES

Transition probabilities are often available in literature or archives. Values from NIST-ASD for here identified spectral lines are reported, together with the other results, in Tables4–35: we will refer to such lines as *reference lines*. For an optically thin plasma, the emission coefficient due to a transition between upper level u and lower level l is (e.g. Kunze 2009)

$$\varepsilon_{\mathrm{ul}} = \frac{h\nu_{\mathrm{ul}}}{4\pi}A_{\mathrm{ul}}n_{\mathrm{u}}, \tag{7}$$

where h is the Planck constant, ν_{ul} is the frequency of the transition, n_{u} the number of emitters at the level u per unit volume, and A_{ul} is the transition probability. After the correction for the relative wavelength sensitivity of the acquisition system, the measured line intensity I_{ul} is proportional to $\varepsilon_{\mathrm{ul}}$ through a constant ϕ that is related to the geometry of the emitting plasma volume. With $\varepsilon_{\mathrm{ul}} = \phi\, I_{\mathrm{ul}}$,

Table 3. Overview of the results. For each element in each ionization stage: $N_{\rm levels}$ is the number of levels used to generate the $N_{\rm Ritz}$ theoretical transitions; $N_{\rm lines}$ is the number of lines observed in each lamp, attributed either to a neutral or ionic transition; $N_{\rm model}$ is the number of lines corresponding to a predicted transition for a given ionization stage; $N_{\rm trans}$ is the number of transitions for which the log *gf* has been estimated; $N_{\rm new}$ is the number of $N_{\rm model}$ lines that are not present in the NIST, Kurucz, or VALD data base for a given element. For $N_{\rm model}$ and $N_{\rm trans}$ also the percentage with respect to $N_{\rm Ritz}$ is reported. For species with determined log *gf* values, the last column lists the most (to our knowledge) recent papers with experimental oscillator strengths to provide the reader of a comparison.

El.	Ion.	$N_{\rm levels}$	$N_{\rm Ritz}$	$N_{\rm lines}$	$N_{\rm model}$ (per cent)	$N_{\rm trans}$ (per cent)	$N_{\rm new}$	Literature
Cs	I	162	348	82	51 (14.7)	0 (0.0)	10	–
	II	298	3728		40 (1.1)	0 (0.0)		–
Ba	I	294	2782	162	154 (5.5)	154 (5.5)	7	Wang et al. (2017)
	II	109	537		13 (2.4)	10 (1.9)		–
Pr	I	407	7171	833	783 (10.9)	0 (0.0)	648	–
	II	191	2788		157 (5.6)	133 (4.8)		Ryder (2011)
Nd	I	708	14 998	1286	1277 (8.5)	1263 (8.4)	927	Ryder (2011)
	II	743	27 235		681 (2.5)	237 (0.9)		Ryder (2011)
Sm	I	472	6339	1527	1216 (19.2)	1207 (19.0)	815	–
	II	376	7312		585 (8.0)	562 (7.7)		Ryder (2011)
Eu	I	381	4995	474	478 (9.6)	478 (9.6)	213	Fan et al. (2014)
	II	140	1521		45 (3.0)	24 (1.6)		Tian et al. (2019)
Gd	I	607	17 645	698	802 (4.5)	594 (3.4)	267	Weeks et al. (2021)
	II	305	5834		94 (1.6)	0 (0.0)		–
Tb	I	586	12 983	2041	2316 (17.8)	0 (0.0)	1941	–
	II	140	1411		81 (5.7)	0 (0.0)		–
Dy	I	707	24 424	726	814 (3.3)	775 (3.2)	356	–
	II	563	18 219		275 (1.5)	48 (0.3)		Biemont & Lowe (1993)
Ho	I	224	2887	373	372 (12.9)	371 (12.9)	292	–
	II	41	158		13 (8.2)	0 (0.0)		–
Er	I	670	18 785	1631	1711 (9.1)	1678 (8.9)	1277	Yu et al. (2019)
	II	360	6050		359 (5.9)	268 (4.4)		Yu et al. (2019)
Tm	I	505	10 957	950	948 (8.7)	944 (8.6)	396	Wang et al. (2022)
	II	361	9453		258 (2.7)	0 (0.0)		–
Yb	I	202	1443	557	325 (22.5)	0 (0.0)	317	–
	II	331	6998		290 (4.1)	0 (0.0)		–
Lu	I	197	2160	45	41 (1.9)	36 (1.7)	14	Fedchak et al. (2000)
	II	36	114		6 (5.3)	0 (0.0)		–
Hf	I	322	6685	816	713 (10.7)	702 (10.5)	131	–
	II	121	957		151 (15.8)	117 (12.2)		Lundqvist et al. (2006)
Re	I	280	3673	88	91 (2.5)	0 (0.0)	43	–
	II	133	306		0 (0.0)	0 (0.0)		–
Os	I	255	3992	339	367 (9.2)	0 (0.0)	134	–
	II	39	57		0 (0.0)	0 (0.0)		–

equation (7) changes to

$$I_{\rm ul} = \frac{h\nu_{\rm ul}}{4\pi}\phi^{-1}A_{\rm ul}n_{\rm u}. \tag{8}$$

Starting from equation (8), expanding the method proposed by Kusz (1992) we are able to determine the $A_{\rm ul}$ value of a transition $u \rightarrow l$ sharing the upper level with (N) reference transitions $u \rightarrow l'$ of which we have here measured the intensities. Writing equation (8) in terms of wavelength and deriving $A_{\rm ul}$ we obtain

$$A_{\rm ul} = \frac{4\pi\phi}{hcn_{\rm u}}\lambda_{\rm ul}I_{\rm ul}. \tag{9}$$

Dividing both members by the product $\lambda_{\rm ul}I_{\rm ul}$ we have

$$\frac{A_{\rm ul}}{\lambda_{\rm ul}I_{\rm ul}} = \frac{4\pi\phi}{hcn_{\rm u}} = \frac{A_{\rm ul'}}{\lambda_{\rm ul'}I'_{\rm ul}}. \tag{10}$$

This relation is valid for each lower level l' for which we observe a transition from u. The quantity $\delta_{\rm u} = 4\pi\phi/(hcn_{\rm u})$ depends only on the upper level u and the constant ϕ, which is related to our instrument. Therefore, using 'exact' quantities the value of $\delta_{\rm u}$ should be exactly equal for all the transitions $u \rightarrow l$, $u \rightarrow l'$, $u \rightarrow l''\ldots$ from the level u. In the real case, the values of $\delta_{\rm u}$ are different, with the differences being of the order of the total uncertainty on $A/(\lambda I)$. If we take the weighted average value of $\delta_{\rm u}$, calculated by our N reference lines and defined by

$$\langle\delta_{\rm u}\rangle = \frac{\sum_{i=1}^{N} w_i \frac{A_{ui}}{\lambda_{ui}I_{ui}}}{\sum_{i=1}^{N} w_i}, \tag{11}$$

where the weights w_i are the inverse squared uncertainties on A_{ui}, we can determine the unknown transition probability $A_{\rm ul}$ by the relation

$$A_{\rm ul} = \lambda_{\rm ul}I_{\rm ul}\langle\delta_{\rm u}\rangle. \tag{12}$$

We will refer to such transition probability estimation method as the *cascade method*.

A transition probability $A_{\rm ul}$ can be also determined by combining equation (8) with the Boltzmann equation,

$$\frac{n_{\rm u}}{\mathcal{N}} = \frac{g_{\rm u}}{U_{\rm I}(T_{\rm e})}\exp\left(-\frac{E_{\rm u}}{k_{\rm B}T_{\rm e}}\right), \tag{13}$$

Table 4. Measured wavelengths (λ_o) and intensities of Cs I spectral lines. Energy level classification is reported as follow: λ_{Ritz} – Ritz wavelength of the transition; E_{up} – energy of the upper level in eV; J_{up} – J of the upper level; E_{low} – energy of the lower level in eV; and J_{low} – J of the lower level. A superscript to observed wavelengths indicates a blend (*b*), a coincidence with a transition of the corresponding ionized state (*c*). In the machine-readable table, full information about the energy levels is reported.

λ_{Ritz} (Å)	E_{up} (eV)	J_{up}	E_{low} (eV)	J_{low}	λ_o (Å)	I (au)
3888.611	3.1874^{o}	0.5	0.0000	0.5	3888.622	68.1
5083.954	3.8239	0.5	1.3859^{o}	0.5	5083.966	49.2
5143.260	3.8645	2.5	1.4546^{o}	1.5	5143.262	18.0
5256.567	3.7438	1.5	1.3859^{o}	0.5	5256.553^{c}	4.9
5413.621	3.7441	2.5	1.4546^{o}	1.5	5413.621	29.6
5465.944	3.6535	1.5	1.3859^{o}	0.5	5465.933	212.7
5502.885	3.7070	2.5	1.4546^{o}	1.5	5502.879	96.0
5503.856	3.7066	1.5	1.4546^{o}	1.5	5503.855	10.1
5568.410	3.6118	0.5	1.3859^{o}	0.5	5568.411	36.2
5573.677	3.6784	0.5	1.4546^{o}	1.5	5573.681	21.0
5635.213	3.6541	2.5	1.4546^{o}	1.5	5635.208	457.8
5636.691	3.6535	1.5	1.4546^{o}	1.5	5636.689	32.0
5664.018	3.5742	1.5	1.3859^{o}	0.5	5664.013	873.5
5745.723	3.6118	0.5	1.4546^{o}	1.5	5745.721	62.8
5838.834	3.5087	0.5	1.3859^{o}	0.5	5838.833	189.3
5845.141	3.5751	2.5	1.4546^{o}	1.5	5845.137	1439.3
5847.572	3.5742	1.5	1.4546^{o}	1.5	5847.569	157.4
6010.490	3.4481	1.5	1.3859^{o}	0.5	6010.489	3344.4
6028.052	3.8538^{o}	1.5	1.7976	1.5	6028.015	742.7
6034.089	3.5087	0.5	1.4546^{o}	1.5	6034.086	240.4

Table 5. Measured wavelengths (λ_o) and intensities of Cs II spectral lines. Meaning of symbols is given in Table 4.

λ_{Ritz} (Å)	E_{up} (eV)	J_{up}	E_{low} (eV)	J_{low}	λ_o (Å)	I (au)
3959.505	16.5096	0.0	13.3793^{o}	1.0	3959.512	63.0
4039.856	18.9499^{o}	3.0	15.8818	2.0	4039.857	38.9
4213.142	18.9499^{o}	3.0	16.0080	3.0	4213.143	8.0
4264.702	18.9143^{o}	4.0	16.0080	3.0	4264.708	95.8
4288.375	19.0077^{o}	2.0	16.1174	1.0	4288.386	34.3
4363.299	19.0543^{o}	3.0	16.2136	2.0	4363.312	40.8
4373.036	16.2136	2.0	13.3793^{o}	1.0	4373.031	61.3
4501.552	16.5096	0.0	13.7562^{o}	1.0	4501.552	416.1
4526.742	16.1174	1.0	13.3793^{o}	1.0	4526.744	126.5
4538.966	18.9443^{o}	2.0	16.2136	2.0	4538.978	28.3
4595.892	21.1975	2.0	18.5006^{o}	2.0	4595.863	29.7
4763.636	17.7741	1.0	15.1722^{o}	0.0	4763.656	24.9
4830.186	15.8818	2.0	13.3158^{o}	2.0	4830.193	213.9
4870.039	17.7793	2.0	15.2342^{o}	1.0	4870.041	60.3
4952.852	15.8818	2.0	13.3793^{o}	1.0	4952.852	475.0
4972.596	18.5006^{o}	2.0	16.0080	3.0	4972.599	42.2
5043.803	16.2136	2.0	13.7562^{o}	1.0	5043.805	688.3
5249.385	16.1174	1.0	13.7562^{o}	1.0	5249.383	114.7
5256.596	18.8676^{o}	1.0	16.5096	0.0	5256.553^{c}	4.9
5370.988	15.6870	1.0	13.3793^{o}	1.0	5370.985	214.0

here k_B is the Boltzmann constant, T_e the electron temperature, g_u ($=2J_u+1$) the energy level degeneracy, $U_I(T_e)=\sum_i \exp\left(-\frac{h\nu_i}{k_B T_e}\right)$ the partition function, and $\mathcal{N}$ the total number of atoms per unit volume. The resulting logarithm relation is

$$\ln\left(\frac{\lambda_{ul} I_{ul}}{g_u A_{ul}}\right) = -\frac{1}{k_B T_e} E_u + \ln\left(\frac{4\pi U_I(T_e)}{h\, c\, \Phi\, \mathcal{N}}\right) \quad (14)$$

at the basis of the so-called *Boltzmann plot*. For a given specie, a linear ($y=\alpha x+\beta$) fit of a set of spectral lines with known transition probabilities (e.g. Fig. 3) straightly gives the transition probability A_{ul} of a spectral line from the measured intensity I_{ul},

$$A_{ul} = \frac{\lambda_{ul} I_{ul}}{g_u} \exp\left(-[\alpha E_u + \beta]\right). \quad (15)$$

Table 6. Measured wavelengths (λ_o) and intensities of Ba I spectral lines. Energy level classification is reported as follow: λ_{Ritz} – Ritz wavelength of the transition; E_{up} – energy of the upper level in eV; J_{up} – J of the upper level; E_{low} – energy of the lower level in eV; and J_{low} – J of the lower level. Last four columns report log gf values of spectral lines: (1) estimated with cascade method (Casc.); (2) estimated with Boltzmann plot method (Boltz.); (3) NIST value for reference lines; and (4) VALD value (if available). A superscript to observed wavelengths indicates a blend (*b*), a coincidence with a transition of the corresponding ionized state (*c*), or the adopted literature log gf (*n*). The (*e*) flag on the Boltzmann log gf indicates an extrapolation from the Boltzmann plot. In the machine-readable table, full information about the energy levels is reported.

λ_{Ritz} (Å)	E_{up} (eV)	J_{up}	E_{low} (eV)	J_{low}	λ_o (Å)	I (au)	Log gf Casc.	Boltz.	NIST-ASD	VALD
3892.655	4.5970	2.0	1.4128^o	2.0	3892.662	91.2		− 1.11 ± 0.23		− 0.510
3909.909	4.2902	1.0	1.1201^o	2.0	3909.903^n	438.1		− 0.70 ± 0.23	− 0.251 ± 0.326	− 0.250
3935.717	4.2919	2.0	1.1426^o	3.0	3935.711^n	749.9		− 0.45 ± 0.23	− 0.117 ± 0.326	− 0.120
3937.868	4.2902	2.0	1.1426^o	2.0	3937.852^n	166.1		− 1.11 ± 0.23	− 0.893 ± 0.326	− 0.900
3993.399	4.2937	3.0	1.1898^o	4.0	3993.397^n	1264.3		− 0.21 ± 0.23	0.073 ± 0.326	0.080
3995.655	4.2919	3.0	1.1898^o	3.0	3995.649^n	40.8		− 1.70 ± 0.23	− 0.831 ± 0.326	− 0.830
4084.867	4.7100^o	2.0	1.6756	3.0	4084.871^e	51.5		− 1.19^e ± 0.23		
4132.427	2.9994	0.0	0.0000^o	1.0	4132.427^n	366.1		− 1.87 ± 0.23	− 1.950 ± 0.043	− 2.000
4179.349	4.6414^o	2.0	1.6756	2.0	4179.350^e	9.8		− 1.94^e ± 0.23		
4223.963	4.4552^o	0.0	1.5208	1.0	4223.957	31.0		− 1.60 ± 0.23		
4239.555	4.5993^o	2.0	1.6756	1.0	4239.548^n	23.3		− 1.58 ± 0.23	− 0.712 ± 0.326	− 0.720
4242.605	4.4883^o	1.0	1.5667	2.0	4242.598^n	15.5		− 1.86 ± 0.23	− 1.122 ± 0.326	− 1.120
4254.348	5.1527^o	1.0	2.2392	1.0	4254.330^e	10.3		− 1.43^e ± 0.23		
4264.417	4.4274^o	0.0	1.5208	1.0	4264.413^n	63.1		− 1.30 ± 0.23	− 0.911 ± 0.326	− 0.900
4283.097	4.3068	2.0	1.4128^o	3.0	4283.097^n	1293.6		− 0.09 ± 0.23	0.091 ± 0.326	0.090
4291.157	4.4552^o	1.0	1.5667	1.0	4291.161	26.8		− 1.64 ± 0.23		
4323.003	4.4339^o	1.0	1.5667	2.0	4323.000^n	124.4		− 0.98 ± 0.23	− 0.909 ± 0.078	− 0.670
4332.914	4.4274^o	1.0	1.5667	1.0	4332.906^n	52.0		− 1.36 ± 0.23	− 0.897 ± 0.326	− 0.890
4350.325	4.4159^o	1.0	1.5667	2.0	4350.319^n	958.7		− 0.10 ± 0.23	− 0.070 ± 0.326	− 0.070
4402.538	4.3821^o	1.0	1.5667	2.0	4402.534^n	918.4		− 0.14 ± 0.23	− 0.406 ± 0.109	0.010

Table 7. Measured wavelengths (λ_o) and intensities of Ba II spectral lines. Meaning of symbols is given in Table 6.

λ_{Ritz} (Å)	E_{up} (eV)	J_{up}	E_{low} (eV)	J_{low}	λ_o (Å)	I (au)	Log gf Casc.	Boltz.	NIST-ASD	VALD
3891.779	5.6970^o	0.5	2.5121	1.5	3891.776^n	494.5		0.56 ± 0.73	0.295 ± 0.043	0.280
4130.649	5.7225^o	1.5	2.7218	2.5	4130.648^n	850.7		0.90 ± 0.73	0.525 ± 0.043	0.680
4166.001	5.6970^o	1.5	2.7218	1.5	4166.000^n	75.8		− 0.16 ± 0.73	− 0.434 ± 0.043	− 0.420
4524.926	5.2514^o	0.5	2.5121	0.5	4524.918^n	240.1		0.04 ± 0.73	− 0.390 ± 0.043	− 0.360
4554.033	2.7218	0.5	0.0000^o	1.5	4554.024^n	31041.9		− 0.13 ± 0.73	0.140 ± 0.043	0.026
4899.927	5.2514^o	1.5	2.7218	0.5	4899.918^n	462.1		0.43 ± 0.73	− 0.126 ± 0.043	− 0.080
4934.077	2.5121	0.5	0.0000^o	0.5	4934.067^n	13100.8		− 0.59 ± 0.73	− 0.158 ± 0.043	− 0.294
5521.735	9.8874^o	1.5	7.6426	1.5	5521.766^e	21.5				
6141.713	2.7218	2.5	0.7036^o	1.5	6141.721^n	1727.8		− 1.00 ± 0.73	− 0.031 ± 0.043	− 0.220
6496.898	2.5121	1.5	0.6043^o	0.5	6496.891^n	1069.0		− 1.32 ± 0.73	− 0.406 ± 0.043	− 0.521
6893.451	9.8070^o	2.5	8.0089	2.5	6893.442^{ce}	8.3				
8515.526	9.8470^o	1.5	8.3914	2.5	8515.562^{ce}	3.5				
8710.768	7.1454	2.5	5.7225^o	3.5	8710.783^n	19.8		1.53 ± 0.73	0.856 ± 0.043	

An example of Boltzmann plot is reported in Fig. 3. The goodness-of-fit coefficient is defined as $R^2 = 1 - \sum_i (y_i - f_i)^2 / \sum_i (y_i - \bar{y})^2$, where y_i are the data with average $\bar{y}$ and f_i the corresponding values from the fit. The method that employs equation (15) hereafter will be called the *Boltzmann method*.

The electron temperatures, obtained with the linear regressions of Boltzmann plots together with their uncertainties, are reported in Table 2. We note that temperatures can be significantly different (e.g. Ba) with the ionization states. It is not clear, if this difference is real or due to the relatively small number of data and their distribution in energy. For example, we found only nine lines (with seven clustered between 2.5 and 2.7 eV plus one line at 2.95 eV and another one at 3.15 eV) for Nd I and 28 for Nd II. As a general rule, for any element we assumed the temperature determined from the largest number of lines. To estimate the uncertainty of log gf, as it is explained in the following subsection, we considered an error in this difference between the temperatures from the two different ionization states.

It should be noted that a transition probability through the cascade method is always correct in the limits of the adopted literature values, while the Boltzmann method is valid only if considered transitions are in thermodynamic equilibrium. As it is pointed out in Kramida, Ryabtsev & Young (2022), if the system is perfectly calibrated for the relative intensity and the values of A_{ul} are exact, the data points on the Boltzmann plot lie on a straight line if the hypothesis of thermodynamic equilibrium is valid. Therefore, even if the HC plasma is not a system in perfect thermodynamic equilibrium, the linearity of the plots (such as Fig. 3) states that this hypothesis is reasonable, at least within the upper energy range of the Boltzmann plots. This is probably due to the fact that the observed plasma region

Table 8. Measured wavelengths (λ_o) and intensities of Pr I spectral lines. Meaning of symbols is given in Table 4.

λ_{Ritz} (Å)	E_{up} (eV)	J_{up}	E_{low} (eV)	J_{low}	λ_o (Å)	I (au)
3924.498	3.1583	4.5	0.0000[o]	4.5	3924.509[b]	37.1
3925.475	3.3281	5.5	0.1707[o]	5.5	3925.457[c]	109.5
3946.191	3.1409	5.5	0.0000[o]	4.5	3946.207	60.1
4001.968	3.2678	5.5	0.1707[o]	5.5	4001.964	13.9
4065.407	3.0488	5.5	0.0000[o]	4.5	4065.417	23.8
4169.653	2.9726	4.5	0.0000[o]	4.5	4169.668	93.2
4214.448	3.1117	5.5	0.1707[o]	5.5	4214.460	39.0
4313.141	3.0444	6.5	0.1707[o]	5.5	4313.154	16.4
4314.675	3.4222[o]	5.5	0.5495	4.5	4314.665	37.1
4320.364	3.4184[o]	5.5	0.5495	4.5	4320.356[c]	43.1
4323.067	3.4704[o]	6.5	0.6034	5.5	4323.066	47.8
4343.390	3.4032[o]	5.5	0.5495	4.5	4343.375	50.1
4360.941	2.8422	4.5	0.0000[o]	4.5	4360.949	23.8
4361.521	2.8418	4.5	0.0000[o]	4.5	4361.523[c]	21.7
4392.445	2.9925	5.5	0.1707[o]	5.5	4392.462	17.1
4395.796	2.8197	5.5	0.0000[o]	4.5	4395.781[c]	63.0
4408.137	3.5337[o]	4.5	0.7219	4.5	4408.147	62.9
4430.125	2.7978	3.5	0.0000[o]	4.5	4430.125	311.7
4441.342	2.7907	4.5	0.0000[o]	4.5	4441.334	16.7
4447.857	3.3362[o]	4.5	0.5495	4.5	4447.858	65.5

is very small (<1 mm) and the thermodynamic equilibrium holds locally. Although effects of non-equilibrium should result in scatter in the plots, increasing the uncertainty on the determined coefficient and, in turn, on the transition probabilities. For transitions with the upper energy level outside the Boltzmann plot range, the log *gf* value is derived from an extrapolation of the line fit and should be taken with caution. Such values are flagged in the table, as we will see in Section 4.

We list line strengths under the form of oscillator strengths, which is the quantity usually taken in input by spectral synthesis codes. Under the electric-dipole transition approximation the oscillator strength is given by (Huber & Sandeman 1986)

$$g_l f_{lu} = 1.49919 \times 10^{-16} \lambda_{ul}^2 g_u A_{ul}, \quad (16)$$

where λ_{ul} is expressed in Å and A_{ul} in s^{-1}. The logarithm of the *gf* expressed in equation (16) is called log *gf* and is the standard form under which line strengths are usually inserted in line lists for spectral synthesis code.

For both methods, the estimate of oscillator strengths of spectral lines relies on the presence of some reference lines in the spectrum with known A_{ul} value. Table 2 resumes all the species for which the estimation of the oscillator strength has been made. In order to maximize the number of ions for which transition probability can be estimated, we decided to take as reference lines those having any uncertainty value on transition probability (from AA to E according to NIST standard). However, in order to mitigate the effect of large uncertainties on reference *A* values, Boltzmann plot fits are weighted with uncertainties and weighted averages are used for the cascade method. If no lines with known oscillator strength are present in the NIST data base, we still decided to estimate transition probabilities, taking reference lines from single studies (Sm I–II, Ho I, Er II, and Hf II) in which experimental determination of log *gf* has been carried out. For some species (reported with '−' in Table 2) the lack of experimental data allowed no estimation of line strengths from our spectra. In such cases, a table with only measured wavelengths, relative intensity, and energy level classification has been compiled.

3.1 Evaluation of the uncertainties

The analysis of the uncertainties on transition probabilities, and in turn on log *gf*, has been carried out to identify the most relevant contributions and evaluate their magnitude. Propagating the uncertainty on equation (16) we obtain

$$\sigma_{\log gf} = \frac{1}{\ln(10)} \sqrt{\frac{4}{\lambda^2}\sigma_\lambda^2 + \frac{1}{A^2}\sigma_A^2}, \quad (17)$$

where the uncertainty on the transition probability σ_A depends on the method used. For the cascade method, using equation (5) to

Table 9. Measured wavelengths (λ_o) and intensities of Pr II spectral lines. Meaning of symbols is given in Table 6.

λ_{Ritz} (Å)	E_{up} (eV)	J_{up}	E_{low} (eV)	J_{low}	λ_o (Å)	I (au)	Log *gf* Casc.	Boltz.	NIST-ASD	VALD
3880.464	3.1942[o]	4.0	0.0000	3.0	3880.486	120.9		−0.33 ± 0.26		−0.489
3885.195	3.3947[o]	6.0	0.2045	5.0	3885.175	66.9		−0.24 ± 0.26		−0.478
3920.532	3.1615[o]	4.0	0.0000	5.0	3920.540	402.4	0.190 ± 0.033	0.15 ± 0.26		−0.943
3925.466	3.1576[o]	4.0	0.0000	4.0	3925.459[n]	109.5		−0.42 ± 0.26	−0.322 ± 0.078	−0.070
3927.463	3.3722[o]	5.0	0.2162	5.0	3927.477	53.2		−0.36 ± 0.26		−0.449
3962.450	3.3443[o]	5.0	0.2162	5.0	3962.444	24.4		−0.74 ± 0.26		−0.090
3982.052	3.5346[o]	6.0	0.4219	6.0	3982.054[e]	178.6		0.46[e] ± 0.26		0.371
3997.040	3.4728[o]	7.0	0.3717	7.0	3997.055[n]	39.1		−0.30 ± 0.26	−0.212 ± 0.043	−0.170
4004.702	3.3113[o]	5.0	0.2162	5.0	4004.696[n]	78.3		−0.27 ± 0.26	−0.249 ± 0.030	−0.302
4015.390	3.3030[o]	5.0	0.2162	5.0	4015.388[n]	60.0		−0.40 ± 0.26	−0.360 ± 0.030	−0.306
4038.455	3.0692[o]	4.0	0.0000	4.0	4038.438	95.3		−0.59 ± 0.26		−0.810
4044.813	3.0644[o]	4.0	0.0000	5.0	4044.785[n]	83.2		−0.66 ± 0.26	−0.295 ± 0.078	−0.282
4054.860	3.2730[o]	5.0	0.2162	6.0	4054.859[n]	240.0		0.16 ± 0.26	0.213 ± 0.078	0.156
4058.800	3.4758[o]	6.0	0.4219	6.0	4058.813[n]	28.2		−0.42 ± 0.26	−0.407 ± 0.043	−0.332
4062.805	3.4728[o]	6.0	0.4219	7.0	4062.814[b]	554.5	0.978 ± 0.040	0.87 ± 0.26		0.570
4062.806	3.4226[o]	7.0	0.3717	6.0	4062.814[b]	645.7		0.85 ± 0.26		
4083.341	3.2517[o]	5.0	0.2162	4.0	4083.334	66.0		−0.42 ± 0.26		−1.380
4096.820	3.2417[o]	5.0	0.2162	5.0	4096.825[n]	90.8		−0.30 ± 0.26	−0.255 ± 0.043	−0.456
4107.507	4.1751	4.0	1.1575[o]	5.0	4107.510[e]	32.3		0.86[e] ± 0.27		−0.734
4129.146	4.0407	5.0	1.0389[o]	5.0	4129.164[e]	39.0		0.72[e] ± 0.27		−0.006

Table 10. Measured wavelengths (λ_o) and intensities of Nd I spectral lines. Meaning of symbols is given in Table 6.

λ_{Ritz} (Å)	E_{up} (eV)	J_{up}	E_{low} (eV)	J_{low}	λ_o (Å)	I (au)	Log gf Casc.	Boltz.	NIST-ASD	VALD
3982.272	3.2524	5.0	0.1399^{o}	4.0	3982.277^{ce}	43.6		$-1.39^{e} \pm 0.16$		
3992.969	3.9428^{o}	6.0	0.8387	7.0	3992.983^{e}	32.4		$-0.63^{e} \pm 0.17$		
4037.633	3.9085^{o}	6.0	0.8387	7.0	4037.643^{e}	34.7		$-0.63^{e} \pm 0.17$		
4053.508	3.1977	5.0	0.1399^{o}	4.0	4053.513^{ce}	36.5		$-1.51^{e} \pm 0.16$		
4066.841	3.0478	4.0	0.0000^{o}	5.0	4066.854	32.2		-1.76 ± 0.16		
4083.896	3.0351	4.0	0.0000^{o}	4.0	4083.904	146.1		-1.11 ± 0.16		
4092.646	3.1684	5.0	0.1399^{o}	5.0	4092.650^{ce}	30.8		$-1.61^{e} \pm 0.16$		
4103.002	3.8596^{o}	6.0	0.8387	5.0	4103.010^{e}	17.8		$-0.96^{e} \pm 0.17$		
4122.980	3.0063	4.0	0.0000^{o}	4.0	4122.979^{c}	38.0		-1.72 ± 0.16		
4126.546	3.1436	5.0	0.1399^{o}	6.0	4126.551	23.4		-1.75 ± 0.16		
4142.016	3.2859	6.0	0.2934^{o}	5.0	4141.995^{e}	10.8		$-1.90^{e} \pm 0.16$		
4160.628	3.2725	6.0	0.2934^{o}	7.0	4160.618^{e}	13.6		$-1.81^{e} \pm 0.16$		
4176.092	3.4245	7.0	0.4565^{o}	7.0	4176.094^{ce}	13.6		$-1.61^{e} \pm 0.16$		
4205.264	3.4040	7.0	0.4565^{o}	6.0	4205.263^{bce}	21.1		$-1.44^{e} \pm 0.16$		
4205.272	3.5734	8.0	0.6259^{o}	8.0	4205.263^{bce}	19.1		$-1.27^{e} \pm 0.16$		
4210.979	3.0833	5.0	0.1399^{o}	5.0	4210.986^{c}	106.1		-1.15 ± 0.16		
4252.949	4.3230^{o}	4.0	1.4086	3.0	4252.967^{e}	20.2		$-0.27^{e} \pm 0.17$		
4256.462	2.9120	4.0	0.0000^{o}	3.0	4256.467^{c}	452.2		-0.72 ± 0.16		-0.790
4258.095	3.0508	5.0	0.1399^{o}	4.0	4258.100	79.0		-1.30 ± 0.16		-1.066
4265.659	3.7444^{o}	6.0	0.8387	5.0	4265.675^{be}	38.9		$-0.72^{e} \pm 0.17$		

Table 11. Measured wavelengths (λ_o) and intensities of Nd II spectral lines. Meaning of symbols is given in Table 6.

λ_{Ritz} (Å)	E_{up} (eV)	J_{up}	E_{low} (eV)	J_{low}	λ_o (Å)	I (au)	Log gf Casc.	Boltz.	NIST-ASD	VALD
3832.897	5.4467^{o}	5.5	2.2129	4.5	3832.879^{e}	224.8				
3858.303	4.4410	3.5	1.2285^{o}	2.5	3858.307^{be}	419.4				
3858.303	3.7627	5.5	0.5502^{o}	6.5	3858.307^{be}	419.4				
3909.230	4.9472^{o}	3.5	1.7765	2.5	3909.258^{e}	77.3				
3920.961	3.5414	5.5	0.3802^{o}	6.5	3920.959	62.4		0.53 ± 0.16		0.010
3924.494	5.2242^{o}	3.5	2.0658	4.5	3924.506^{e}	26.7				
3941.506	3.2084	4.5	0.0636^{o}	4.5	3941.519	123.2		0.41 ± 0.16		−0.020
3945.406	5.5914^{o}	4.5	2.4497	3.5	3945.380^{e}	23.6				
3951.142	3.3193	5.5	0.1823^{o}	5.5	3951.145^{n}	43.3		0.10 ± 0.16	0.043 ± 0.030	0.040
3952.188	3.1362	3.5	0.0000^{o}	3.5	3952.189^{n}	21.3		−0.44 ± 0.16	−0.395 ± 0.030	−0.390
3957.993	3.1953	4.5	0.0636^{o}	4.5	3958.006	30.4		−0.21 ± 0.16		−0.670
3963.105	3.5990	7.5	0.4714^{o}	8.5	3963.100^{n}	21.7		0.16 ± 0.16	0.227 ± 0.030	0.230
3963.326	4.2081	1.5	1.0807^{o}	1.5	3963.356^{e}	44.7				
3978.706	4.8573	5.5	1.7420^{o}	6.5	3978.733^{e}	33.5				
3982.257	4.7304	5.5	1.6178^{o}	4.5	3982.277^{ce}	43.6				
3988.802	3.4877	5.5	0.3802^{o}	5.5	3988.818	29.4		0.16 ± 0.16		−1.240
3990.097	3.5778	7.5	0.4714^{o}	7.5	3990.093^{n}	14.1		−0.04 ± 0.16	0.135 ± 0.030	0.130
3991.741	3.1051	3.5	0.0000^{o}	3.5	3991.743^{n}	23.1		−0.44 ± 0.16	−0.258 ± 0.030	−0.260
3994.454	4.5944^{o}	6.5	1.4913	5.5	3994.452^{be}	34.2				
3994.457	5.0149^{o}	1.5	1.9119	1.5	3994.452^{be}	34.2				

propagate errors on equation (12) we have

$$\sigma_A = \sqrt{I_{ul}^2 < \delta_u >^2 \sigma_{\lambda_{ul}}^2 + \lambda_{ul}^2 < \delta_u >^2 \sigma_{I_{ul}}^2 + \lambda_{ul}^2 I_{ul}^2 \sigma_{\langle\delta_u\rangle}^2}, \quad (18)$$

where the uncertainty on $\langle\delta_u\rangle$ is obtained propagating the uncertainties on A, λ, and I through the weighted average. For log gf estimated with the Boltzmann method, the main contribution to the uncertainty is due to the difference between reference transition probabilities and those calculated through the fit. An example of this difference, shown as a relative difference, is reported in Fig. 4 for Nd II lines. For each of the elements with log gf estimated through the Boltzmann method, we identified the best estimation of the uncertainty as the standard deviation of the quantity $dA_{rel} = (A_{ref} - A_{Boltz})/A_{ref}$, which is about 30 per cent in the case of Nd II. Therefore, the value of σ_A used in equation (17) is equal to $\sigma_A = dA_{rel} A_{Boltz}$. In order to evaluate the uncertainty due to the temperature differences between the two lamps, a 'sensitivity study' on the derivation of the Boltzmann plot and log gf has been carried out for the ions with constrained temperature. The fit has been made constraining the temperature both with the neutral and the ion temperature, evaluating the difference in the obtained log gf: Such difference has been taken as an additional uncertainty on the log gf and has been summed in quadrature to the other uncertainties.

Table 12. Measured wavelengths (λ_o) and intensities of Sm I spectral lines. Meaning of symbols is given in Table 6.

λ_{Ritz}	E_{up}	J_{up}	E_{low}	J_{low}	λ_o	I	Log gf			
(Å)	(eV)		(eV)		(Å)	(au)	Casc.	Boltz.	Lawler, Fittante & Den Hartog (2013)	VALD
3773.339	3.3211	1.0	0.0363	2.0	3773.339[n]	973.2		−1.10 ± 0.26	−0.629 ± 0.026	−0.887
3793.977	3.6545	5.0	0.3875[o]	5.0	3793.990[c]	539.7		−0.88 ± 0.26		
3803.941	3.2584	0.0	0.0000	1.0	3803.942[n]	1059.2		−1.14 ± 0.26	−0.755 ± 0.023	−0.826
3806.450	3.7548	6.0	0.4985[o]	5.0	3806.479	505.0	−0.716 ± 0.072	−0.77 ± 0.26		−0.610
3809.957	3.6408	5.0	0.3875	4.0	3809.954[n]	1460.9		−0.46 ± 0.26	−0.565 ± 0.022	−0.288
3813.825	3.7485	6.0	0.4985	5.0	3813.824[n]	1322.9		−0.35 ± 0.26	−0.319 ± 0.024	−0.099
3822.961	3.3429	2.0	0.1007	1.0	3822.966[n]	439.5		−1.39 ± 0.26	−1.248 ± 0.025	−1.246
3826.239	3.5213	4.0	0.2818[o]	4.0	3826.215[c]	345.5		−1.25 ± 0.26		
3832.805	3.5157	4.0	0.2818	3.0	3832.806[n]	1872.0		−0.52 ± 0.26	−0.691 ± 0.023	−0.623
3834.475	3.7310	6.0	0.4985	6.0	3834.473[n]	4311.6		0.14 ± 0.26	0.206 ± 0.022	0.403
3846.282	3.3232	2.0	0.1007	1.0	3846.279[n]	987.8		−1.06 ± 0.26	−1.060 ± 0.023	−1.046
3848.782	3.3211	2.0	0.1007	2.0	3848.788[n]	734.0		−1.19 ± 0.26	−0.977 ± 0.059	
3853.296	3.6042	5.0	0.3875	5.0	3853.295[n]	2670.3		−0.24 ± 0.26	−0.335 ± 0.028	−0.172
3854.578	3.4003	3.0	0.1847	3.0	3854.577[n]	1035.6		−0.93 ± 0.26	−0.617 ± 0.025	−0.621
3858.505	3.3130	2.0	0.1007[o]	2.0	3858.521[bc]	1174.5	−1.075 ± 0.023	−1.00 ± 0.26		
3858.513	3.3970	3.0	0.1847[o]	2.0	3858.521[bc]	1225.7		−0.86 ± 0.26		−0.131
3858.736	3.4940	4.0	0.2818	4.0	3858.739[n]	2669.5		−0.39 ± 0.26	−0.236 ± 0.023	0.288
3860.133	3.5985	5.0	0.3875[o]	5.0	3860.152	3302.5		−0.15 ± 0.26		
3877.467	3.6951	6.0	0.4985	6.0	3877.466[n]	3091.3		−0.04 ± 0.26	−0.151 ± 0.022	0.003
3883.989	3.5788	5.0	0.3875[o]	6.0	3884.002[c]	212.8		−1.36 ± 0.26		

Table 13. Measured wavelengths (λ_o) and intensities of Sm II spectral lines. Meaning of symbols is given in Table 6.

λ_{Ritz}	E_{up}	J_{up}	E_{low}	J_{low}	λ_o	I	Log gf			
(Å)	(eV)		(eV)		(Å)	(au)	Casc.	Boltz.	Lawler et al. (2006)	VALD
3826.207	3.7833	4.5	0.5438	4.5	3826.209[n]	261.1		−0.30 ± 0.14	−0.192 ± 0.022	−0.190
3848.814	3.4087	0.5	0.1882[o]	1.5	3848.794[c]	725.5		−0.37 ± 0.14		
3851.880	3.4954	4.5	0.2775[o]	4.5	3851.894	147.7	−0.968 ± 0.024	−0.94 ± 0.14		−1.030
3853.290	3.5952	5.5	0.3785[o]	4.5	3853.301[c]	2670.3		0.46 ± 0.14		
3854.204	3.8752	5.5	0.6593	5.5	3854.196[n]	704.4		0.27 ± 0.14	0.139 ± 0.022	0.140
3855.903	3.2550	1.5	0.0405	0.5	3855.901[n]	121.4		−1.36 ± 0.14	−0.923 ± 0.023	−0.920
3858.522	4.6580	2.5	1.4456[o]	1.5	3858.521[ce]	1225.7				
3871.784	3.3860	3.5	0.1846[o]	4.5	3871.784	234.9	−0.816 ± 0.014	−0.88 ± 0.14		−0.740
3881.379	3.5268	2.5	0.3334	3.5	3881.387[n]	129.3		−0.94 ± 0.14	−0.965 ± 0.029	−0.960
3882.865	3.6260	3.5	0.4338[o]	3.5	3882.858	134.6		−0.79 ± 0.14		−1.760
3883.988	3.6251	3.5	0.4338[o]	2.5	3884.002[c]	212.8		−0.59 ± 0.14		
3885.278	3.6750	6.5	0.4847	6.5	3885.284[n]	1186.4		0.23 ± 0.14	0.057 ± 0.023	0.060
3890.078	3.3709	3.5	0.1846[o]	3.5	3890.091	139.9	−1.220 ± 0.017	−1.12 ± 0.14		−0.950
3891.185	3.3736	0.5	0.1882[o]	0.5	3891.181[b]	132.6	−1.025 ± 0.023	−1.14 ± 0.14		−1.320
3891.205	4.3521	2.5	1.1667[o]	3.5	3891.181[be]	132.6		0.22[e] ± 0.15		
3896.972	3.2211	1.5	0.0405	2.5	3896.965[n]	423.7		−0.85 ± 0.14	−0.669 ± 0.022	−0.670
3903.416	3.4529	4.5	0.2775[o]	4.5	3903.415	359.0		−0.60 ± 0.14		−0.608
3917.435	3.2680	2.5	0.1039	2.5	3917.435[n]	200.6		−1.10 ± 0.14	−1.003 ± 0.024	−1.000
3922.386	3.5385	5.5	0.3785	5.5	3922.392[n]	666.1		−0.20 ± 0.14	−0.259 ± 0.022	−0.260
3928.275	3.3399	3.5	0.1846	3.5	3928.278[n]	605.3		−0.52 ± 0.14	−0.548 ± 0.023	−0.550

4 RESULTS

Results are reported in tables containing the measured quantities, which are observed wavelengths and relative intensities. In addition they list configuration, term information (when available), J value, parity and energy of the upper and lower levels from NIST-ADS. These machine-readable tables are available in the electronic version of the paper. Tables 4–35 are extracted from the complete tables containing line data. If possible, the values of log gf obtained using the Boltzmann method and/or the cascade method are also given, with the VALD ones. The uncertainties on the log gf mostly depend on the reference values used to calculate A_{ul} with equation (12) or the Boltzmann plot coefficients. Typical values for uncertainties on log gf are included in the range 0.1–0.5, with the exception of Ba II values having uncertainties of 0.7 due to uncertainty about the temperature (see Table 7).

We decided not to report log gf values when exceeding the 'threshold' value of 1.00, except for reference lines. Such a large value is typical only of very intense lines, a log gf value greater than 1.00 is probably due to (a) a transition for which local thermodynamic equilibrium (LTE) does not hold; (b) coincidence (or blend) with transitions resulting in an overestimation of the line intensity.

For most elements, the lines of the neutral state are much more numerous than the lines of the ionized state. This is mainly for two reasons: (a) in HC lamps operating at standard current (and therefore

Table 14. Measured wavelengths (λ_o) and intensities of Eu I spectral lines. Meaning of symbols is given in Table 6.

λ_{Ritz} (Å)	E_{up} (eV)	J_{up}	E_{low} (eV)	J_{low}	λ_o (Å)	I (au)	Casc.	Log gf Boltz.	NIST-ASD	VALD
3884.741	4.9963	4.5	1.8057^o	3.5	3884.751^e	259.2		0.00^e ± 0.23		0.620
3900.510	4.8171^o	4.5	1.6393	5.5	3900.512^e	261.6		−0.19^e ± 0.23		0.110
3949.613	4.7561^o	3.5	1.6179	4.5	3949.601^e	62.7		−0.86^e ± 0.23		−0.110
3955.746	5.0653	5.5	1.9319^o	4.5	3955.763^e	101.5		−0.31^e ± 0.23		0.200
3961.116	4.8733	3.5	1.7442^o	4.5	3961.131^e	22.9		−1.16^e ± 0.23		
3964.477	4.8707	3.5	1.7442^o	3.5	3964.491^e	73.1		−0.66^e ± 0.23		
3964.930	4.7440^o	3.5	1.6179	4.5	3964.943^e	41.6		−1.05^e ± 0.23		
3967.169	4.8686	3.5	1.7442^o	2.5	3967.181^e	86.4		−0.59^e ± 0.23		−0.120
3969.222	5.0546	5.5	1.9319^o	4.5	3969.220^e	70.2		−0.47^e ± 0.23		
3978.402	5.5285^o	2.5	2.4130	2.5	3978.420^{be}	89.1		0.16^e ± 0.23		
3978.417	4.7840^o	5.5	1.6685	6.5	3978.420^{be}	89.1		−0.67^e ± 0.23		−0.070
4004.578	5.5063^o	5.5	2.4111	4.5	4004.552^{ce}	25.8		−0.40^e ± 0.23		
4010.412	4.6930^o	2.5	1.6023	3.5	4010.420^e	122.9		−0.62^e ± 0.23		
4010.432	4.8963	4.5	1.8057^o	4.5	4010.420^e	84.4		−0.56^e ± 0.23		
4016.691	4.6882^o	2.5	1.6023	3.5	4016.698^e	181.2		−0.45^e ± 0.23		
4026.503	4.9903^o	3.5	1.9120	4.5	4026.490^e	20.6		−1.06^e ± 0.23		
4029.957	5.4653^o	4.5	2.3896	3.5	4029.972^{be}	122.6		0.24^e ± 0.23		
4029.968	5.4766^o	3.5	2.4009	4.5	4029.972^{be}	122.6		0.26^e ± 0.23		
4029.973	4.7840^o	6.5	1.7083	6.5	4029.972^{be}	120.0		−0.52^e ± 0.23		
4029.986	4.7840^o	6.5	1.7083	7.5	4029.972^{be}	120.0		−0.52^e ± 0.23		

Table 15. Measured wavelengths (λ_o) and intensities of Eu II spectral lines. Meaning of symbols is given in Table 6.

λ_{Ritz} (Å)	E_{up} (eV)	J_{up}	E_{low} (eV)	J_{low}	λ_o (Å)	I (au)	Casc.	Log gf Boltz.	NIST-ASD	VALD
3866.753	4.4555^o	3.0	1.2500	4.0	3866.742^e	281.9		0.25^e ± 0.09		
3907.106	3.3794^o	3.0	0.2070	2.0	3907.108^n	3221.2		0.13 ± 0.09	0.195 ± 0.003	−0.112
3930.499	3.3605^o	3.0	0.2070	3.0	3930.493^n	4895.2		0.30 ± 0.09	0.239 ± 0.004	−0.012
3971.972	3.3275^o	3.0	0.2070	4.0	3971.972^n	5921.6		0.36 ± 0.09	0.277 ± 0.005	−0.012
4004.176	6.8385	2.0	3.7430^o	3.0	4004.187^e	51.1				
4004.583	4.3451^o	3.0	1.2500	4.0	4004.552^{ce}	25.8		−0.86^e ± 0.09		
4011.680	6.0911	4.0	3.0014^o	4.0	4011.674^e	59.7				0.390
4017.585	4.4048^o	5.0	1.3196	4.0	4017.578^e	14.9		−1.03^e ± 0.09		−1.250
4129.725	3.0014^o	4.0	0.0000	4.0	4129.719^n	8835.3		0.22 ± 0.09	0.194 ± 0.006	−0.062
4205.042	2.9476^o	4.0	0.0000	3.0	4205.040^n	9872.7		0.24 ± 0.09	0.120 ± 0.006	−0.072
4329.984	6.7682	3.0	3.9056^o	3.0	4329.972^{ce}	252.2				
4355.087	6.0911	5.0	3.2450^o	4.0	4355.088^e	68.2				0.630
4435.578	3.0014^o	3.0	0.2070	4.0	4435.573^n	3054.7		−0.14 ± 0.09	−0.085 ± 0.014	−0.392
4522.581	2.9476^o	3.0	0.2070	3.0	4522.576^n	843.7		−0.74 ± 0.09	−0.673 ± 0.004	−0.952
4762.937	4.7106^o	4.0	2.1082	4.0	4762.919^{ce}	40.5		−0.04^e ± 0.09		
4769.636	6.7423	5.0	4.1436^o	4.0	4769.619^{ce}	29.1				
4867.557	6.8385	4.0	4.2921^o	3.0	4867.583^{ce}	848.1				
5089.096	6.9795	5.0	4.5439^o	4.0	5089.063^{ce}	243.0				
5129.128	7.3207	4.0	4.9041^o	3.0	5129.087^{ce}	1553.0				
5169.739	7.1006	5.0	4.7030^o	4.0	5169.734^{ce}	40.7				

temperatures) there are much more neutrals than ions, and therefore neutral lines are much more intense and prevalent; (b) except for Cs, Nd, and Yb, more levels for the neutrals are known rather than for ions (see Table 3); for this reason, since our identification process is based upon the knowledge of theoretical transitions, few energy levels lead to few theoretical lines and, consequently, few observed spectral lines. A superscript to wavelengths indicates a blend (*b*), a coincidence with a transition of the corresponding ionized state (*c*), or the adopted literature log gf (*n*). The superscript (*e*) to log gf indicates that the value is due to an extrapolation of the Boltzmann plot outside the LTE energy range.

An example of comparison between Boltzmann and cascade values is reported in Fig. 5 for Nd II lines. Boltzmann plots (top panel) and comparisons with reference values (bottom panel) are given in Figs 6–24, where the average of the differences between the reference log gf values and the Boltzmann values is ≃0 for almost all elements, with standard deviations ranging from 0.05 to 0.6. For many species, a negative systematic difference between Boltzmann and reference log gf for redder lines ($\lambda > 6000$ Å) is present. Figure 5 shows the agreement between the Boltzmann and cascade values is reasonable considering the uncertainties, which are the sum in quadrature of the two uncertainties for the two methods. As can be seen from the complete tables, similar values are obtained for the other elements.

Table 3 resumes the results in terms of an overall number of lines measured for each element and species (neutral or singly ionized). N_{levels} is the number of energy levels used to calculate

Table 16. Measured wavelengths (λ_o) and intensities of Gd I spectral lines. Meaning of symbols is given in Table 6.

λ_{Ritz} (Å)	E_{up} (eV)	J_{up}	E_{low} (eV)	J_{low}	λ_o (Å)	I (au)	Log gf Casc.	Boltz.	NIST-ASD	VALD
3843.272	3.4382[o]	6.0	0.2131	5.0	3843.277[e]	607.8		0.06[e] ± 0.10		0.114
3866.989	3.4185[o]	6.0	0.2131	5.0	3866.988[ce]	638.0		0.06[e] ± 0.10		0.078
3887.735	3.2543[o]	4.0	0.0661	3.0	3887.750[e]	46.8		−1.37[e] ± 0.10		−1.275
3902.716	3.2998[o]	5.0	0.1239	5.0	3902.720[e]	275.6		−0.51[e] ± 0.10		−0.658
3905.647	3.3867[o]	6.0	0.2131	5.0	3905.654[e]	289.6		−0.33[e] ± 0.10		−0.439
3934.787	3.2162[o]	4.0	0.0661	5.0	3934.787[e]	395.3		−0.49[e] ± 0.10		−0.374
3935.388	3.1496[o]	2.0	0.0000	3.0	3935.385[c]	111.1		−1.17 ± 0.10		−1.000
3940.675	5.0992[o]	3.0	1.9538	4.0	3940.679[e]	60.9				
3941.797	3.3576[o]	6.0	0.2131	6.0	3941.797[e]	323.4		−0.32[e] ± 0.10		−0.480
3943.236	3.1433[o]	2.0	0.0000	1.0	3943.235	248.2		−0.82 ± 0.10		−0.910
3945.532	3.2654[o]	5.0	0.1239	6.0	3945.544[be]	615.7		−0.21[e] ± 0.10		−0.070
3945.563	3.1415[o]	2.0	0.0000	2.0	3945.544[b]	600.9		−0.44 ± 0.10		
3953.366	3.2014[o]	4.0	0.0661	4.0	3953.371[e]	193.7		−0.82[e] ± 0.10		−0.541
3958.674	3.1311[o]	2.0	0.0000	3.0	3958.684	47.8		−1.56 ± 0.10		−1.222
3960.108	3.9949[o]	5.0	0.8650	6.0	3960.113[e]	93.7		0.30[e] ± 0.11		0.059
3966.276	3.3382[o]	6.0	0.2131	7.0	3966.276[be]	309.2		−0.37[e] ± 0.10		−0.273
3966.280	5.0788[o]	3.0	1.9538	4.0	3966.276[be]	309.2				
3968.999	3.1496[o]	3.0	0.0267	3.0	3969.001	319.6		−0.69 ± 0.10		−0.447
3972.706	3.1200[o]	2.0	0.0000	2.0	3972.710	184.9		−0.98 ± 0.10		−0.721
3974.812	3.3315[o]	6.0	0.2131	7.0	3974.813[ce]	101.4		−0.86[e] ± 0.10		−0.544

Table 17. Measured wavelengths (λ_o) and intensities of Gd II spectral lines. Meaning of symbols is given in Table 4.

λ_{Ritz} (Å)	E_{up} (eV)	J_{up}	E_{low} (eV)	J_{low}	λ_o (Å)	I (au)
3866.996	4.7892	2.5	1.5840[o]	2.5	3866.988[b]	638.0
3881.844	3.6200	2.5	0.4270[o]	3.5	3881.867	741.9
3894.693	3.1824	3.5	0.0000[o]	2.5	3894.719	108.1
3935.399	5.4996	1.5	2.3501[o]	2.5	3935.385[c]	111.1
3974.790	5.3954[o]	6.5	2.2771	7.5	3974.812[c]	106.2
3984.127	5.6022[o]	4.5	2.4912	5.5	3984.149	31.0
4033.261	5.3903[o]	4.5	2.3172	5.5	4033.273[c]	19.0
4035.396	5.2996	2.5	2.2281[o]	2.5	4035.395[c]	168.1
4080.552	6.1112	3.5	3.0737[o]	2.5	4080.524[c]	112.0
4085.558	3.7649	5.5	0.7311[o]	6.5	4085.573	28.2
4094.475	3.5495	2.5	0.5223[o]	2.5	4094.486	13.1
4098.599	3.8430	6.5	0.8189[o]	7.5	4098.610	55.8
4130.352	3.6011	4.5	0.6002[o]	5.5	4130.371[b]	31.9
4130.366	3.7320	5.5	0.7311[o]	6.5	4130.371[b]	30.7
4132.264	3.6011	4.5	0.6016[o]	4.5	4132.278	14.9
4163.087	3.6393	6.5	0.6620[o]	5.5	4163.108	41.2
4184.258	3.4547	5.5	0.4925[o]	4.5	4184.259	42.3
4204.858	3.4700	3.5	0.5223[o]	2.5	4204.861	12.9
4212.006	4.3895[o]	2.5	1.4468	2.5	4212.015[b]	25.4
4212.010	3.3676	4.5	0.4249[o]	3.5	4212.015[bc]	25.4

the theoretical transitions for a given species. N_{Ritz} is the number of transitions obtained in our spectral range fulfilling the electric-dipole selection rules. N_{lines} is the number of spectral lines measured for that lamp. N_{model} represents the number of transitions for the given state that are compatible with one of the observed lines. Often differences in energy between electron transitions are so small to let doubtful the identification of the two atomic configurations and terms responsible of the observed spectral line. Even more, it can be impossible to state if a spectral line is from a neutral atom or its ionized state. For this reason, the sum of N_{model} for neutral and ion may be greater than N_{lines}. N_{trans} is the number of transitions for which the log gf has been estimated. Finally, N_{new} is the number of observed lines that is not present in any of the three main data bases: the NIST data base, the Kurucz data base, and VALD. Considering the average values, the 10 per cent and the 5 per cent of the Ritz transitions have been identified in the spectra for neutrals and singly ionized, respectively. The number of lines not previously listed in the NIST+VALD+Kurucz data bases is about 7700: for a lot of lamps this number is several hundred, it is greater than 1000 for Tb and Er.

This research is based on the NIST data base to have a solid reference system. Primarily because of three reasons, it is quite difficult to compare our massive results with literature values and highlight possible systematic differences: (1) according to the SAO/NASA Astrophysics Data System, many thousands of papers have the string

Table 18. Measured wavelengths (λ_o) and intensities of Tb I spectral lines. Meaning of symbols is given in Table 4.

λ_{Ritz} (Å)	E_{up} (eV)	J_{up}	E_{low} (eV)	J_{low}	λ_o (Å)	I (au)
3759.342	3.6491[o]	4.5	0.3521	4.5	3759.338[b]	10155.8
3760.023	3.4664[o]	5.5	0.1700	4.5	3760.033	2567.2
3763.969	4.0805[o]	5.5	0.7875	6.5	3763.974	594.2
3765.116	3.4619[o]	4.5	0.1700	4.5	3765.124	4370.5
3769.266	3.3237[o]	5.5	0.0354	6.5	3769.279	1282.7
3791.055	3.6216[o]	4.5	0.3521	4.5	3791.068	951.7
3792.200	3.9322[o]	4.5	0.6637	5.5	3792.225[b]	1250.5
3792.222	3.5684[o]	4.5	0.3000	3.5	3792.225[b]	1426.4
3794.184	3.7279[o]	7.5	0.4612	6.5	3794.196	646.1
3796.242	3.7261[o]	5.5	0.4612	6.5	3796.259	3743.1
3797.005	3.9871[o]	3.5	0.7228	4.5	3797.016	743.9
3799.578	3.8382[o]	7.5	0.5761	8.5	3799.555	659.3
3799.918	3.6554[o]	2.5	0.3936	2.5	3799.943	791.9
3801.421	3.3237[o]	5.5	0.0632	5.5	3801.423	1981.8
3804.433	3.3211[o]	6.5	0.0632	5.5	3804.438	4675.1
3817.806	3.5465[o]	3.5	0.3000	3.5	3817.816	486.8
3821.407	3.4134[o]	3.5	0.1700	4.5	3821.423	715.4
3824.226	3.7022[o]	5.5	0.4612	6.5	3824.242	410.1
3824.466	3.7020[o]	7.5	0.4612	6.5	3824.459	2704.8
3826.793	3.9026[o]	4.5	0.6637	5.5	3826.812	441.9

Table 19. Measured wavelengths (λ_o) and intensities of Tb II spectral lines. Meaning of symbols is given in Table 4.

λ_{Ritz} (Å)	E_{up} (eV)	J_{up}	E_{low} (eV)	J_{low}	λ_o (Å)	I (au)
3887.880	4.6526[o]	6.0	1.4646	7.0	3887.876[b]	2487.1
3887.898	4.0041[o]	5.0	0.8162	5.0	3887.876[bc]	2488.7
3893.359	3.6079[o]	7.0	0.4244	8.0	3893.367	121.7
3909.537	3.9419[o]	7.0	0.7716	7.0	3909.556[c]	1523.5
3913.770	4.6099[o]	7.0	1.4430	6.0	3913.780	708.6
3916.945	4.1907[o]	6.0	1.0263	5.0	3916.953[c]	758.0
3919.505	3.9524	6.0	0.7901[o]	6.0	3919.512	217.3
3925.428	3.7987	6.0	0.6412[o]	6.0	3925.434	699.3
3940.652	3.2713	7.0	0.1260[o]	7.0	3940.620	391.1
3946.890	3.5135	6.0	0.3732[o]	7.0	3946.890[c]	419.1
3986.330	3.7474[o]	7.0	0.6382	6.0	3986.345	84.1
4004.209	3.9524	6.0	0.8570[o]	5.0	4004.231	311.9
4012.723	3.7379	5.0	0.6490[o]	5.0	4012.738	190.1
4020.469	3.8142[o]	6.0	0.7313	6.0	4020.495	928.1
4031.625	3.5135	6.0	0.4392[o]	6.0	4031.632	368.9
4036.702	3.7086[o]	6.0	0.6382	6.0	4036.725	209.1
4066.174	3.8198[o]	8.0	0.7716	7.0	4066.188	205.9
4103.912	3.1462	7.0	0.1260[o]	7.0	4103.916	807.2
4109.558	4.3997[o]	7.0	1.3837	8.0	4109.531	33.9
4134.401	4.6832[o]	7.0	1.6853	8.0	4134.392[c]	1199.4

'oscillator strength' in their title or abstract; (2) most of these papers are focused on a relatively small numbers of spectral lines; and (3) available experimental oscillator strengths are based on different methods. Table 3 reports the most recent (according to) references with experimental oscillator strengths that the reader can compare to our results if interested in given lines. As an example, we found that for the 18 spectral lines of Ba I in common with Wang et al. (2017) the difference is $\log gf_{our} - \log gf_{Wang} = -0.05 \pm 0.38$. In addition, we report our $\log gf$ versus literature values of the first unblended spectral line in common:

(1) Ba I 4132.427 Å: $\log gf = -1.95 \pm 0.23$ versus -1.90 (Wang et al. 2017);

(2) Pr II 4535.923 Å: $\log gf = -0.45 \pm 0.25$ versus -0.76 (Ryder 2011);

(3) Nd I 5887.874 Å: $\log gf = -1.07 \pm 0.15$ versus -1.23 (Ryder 2011);

(4) Nd II 5092.794 Å: $\log gf = -0.49 \pm 0.16$ versus -0.74 (Ryder 2011);

(5) Sm II 4719.841 Å: $\log gf = 1.05 \pm 0.14$ versus -1.136 (Ryder 2011);

(6) Eu I 5967.114 Å: $\log gf = 0.44 \pm 0.23$ versus 0.40 (Fan et al. 2014);

(7) Eu II 3819.672 Å: $\log gf = 0.485 \pm 0.003$ versus 0.52 (Tian et al. 2019);

Table 20. Measured wavelengths (λ_o) and intensities of Dy I spectral lines. Meaning of symbols is given in Table 6.

λ_{Ritz} (Å)	E_{up} (eV)	J_{up}	E_{low} (eV)	J_{low}	λ_o (Å)	I (au)	Casc.	Log gf Boltz.	NIST-ASD	VALD
3832.896	4.8029^{o}	7.0	1.5690	7.0	3832.872^{ce}	526.0				
3840.890	4.2833^{o}	7.0	1.0562	6.0	3840.890	181.9		−0.10 ± 0.22		
3847.019	4.1600^{o}	8.0	0.9380	7.0	3847.030	253.4		−0.12 ± 0.22		0.465
3868.805	4.1418^{o}	8.0	0.9380	8.0	3868.799^{n}	1080.3		0.49 ± 0.22	1.073 ± 0.217	1.035
3874.052	4.2557^{o}	7.0	1.0562	7.0	3874.042	152.8		−0.20 ± 0.22		
3883.313	4.6805^{o}	8.0	1.4887	9.0	3883.321^{e}	79.1		0.08^{e} ± 0.22		
3891.967	4.1228^{o}	8.0	0.9380	9.0	3891.980	232.8		−0.19 ± 0.22		
3892.880	4.8573^{o}	9.0	1.6733	10.0	3892.910^{be}	259.6		0.84^{e} ± 0.22		
3892.899	4.1220^{o}	8.0	0.9380	8.0	3892.910^{b}	259.2		−0.14 ± 0.22		0.267
3894.530	4.6713^{o}	8.0	1.4887	8.0	3894.532^{e}	33.2		−0.30^{e} ± 0.22		0.266
3896.646	4.4318^{o}	6.0	1.2509	6.0	3896.661^{ce}	53.5		−0.42^{e} ± 0.22		
3913.621	4.1051^{o}	8.0	0.9380	7.0	3913.641^{b}	102.5		−0.56 ± 0.22		−0.044
3913.647	5.2020^{o}	4.0	2.0349	4.0	3913.641^{be}	103.0		0.90^{e} ± 0.22		
3917.286	4.1022^{o}	8.0	0.9380	9.0	3917.308	651.1		0.24 ± 0.22		0.540
3919.121	4.6100^{o}	6.0	1.4473	5.0	3919.152^{be}	97.7		0.09^{e} ± 0.22		
3919.153	4.2189^{o}	7.0	1.0562	7.0	3919.152^{b}	62.7		−0.62 ± 0.22		
3927.858	4.6030^{o}	6.0	1.4473	6.0	3927.873^{e}	80.2		−0.00^{e} ± 0.22		0.930
3930.127	5.7518^{o}	7.0	2.5980	7.0	3930.150^{bce}	183.7				
3930.145	4.7523^{o}	10.0	1.5985	10.0	3930.150^{bce}	186.1		0.56^{e} ± 0.22		1.190
3936.699	4.3873^{o}	9.0	1.2387	10.0	3936.706^{e}	218.0		0.15^{e} ± 0.22		0.719

Table 21. Measured wavelengths (λ_o) and intensities of Dy II spectral lines. Meaning of symbols is given in Table 6.

λ_{Ritz} (Å)	E_{up} (eV)	J_{up}	E_{low} (eV)	J_{low}	λ_o (Å)	I (au)	Casc.	Log gf Boltz.	NIST-ASD	VALD
3841.310	3.3294	7.5	0.1027^{o}	6.5	3841.330	761.7		0.61 ± 0.34		−0.780
3872.104	3.2011	8.5	0.0000^{o}	8.5	3872.107^{n}	252.8		−0.03 ± 0.34	0.012 ± 0.002	0.010
3887.084	5.8091^{o}	6.5	2.6204	7.5	3887.066^{e}	55.0				
3889.700	6.2014^{o}	8.5	3.0148	9.5	3889.681^{e}	153.7				
3896.671	6.3386^{o}	6.5	3.1577	7.5	3896.661^{ce}	57.2				
3898.529	3.7690	6.5	0.5896^{o}	7.5	3898.531^{n}	144.1		0.50 ± 0.34	0.233 ± 0.001	0.230
3930.171	6.4120^{o}	9.5	3.2583	8.5	3930.150^{ce}	201.7				
3944.680	3.1422	8.5	0.0000^{o}	8.5	3944.679^{n}	249.3		−0.09 ± 0.34	0.110 ± 0.001	0.110
3953.537	5.3168^{o}	6.5	2.1817	6.5	3953.509^{ce}	89.2				
3962.609	5.8770^{o}	6.5	2.7491	5.5	3962.594^{ce}	221.8				
3967.530	5.9577^{o}	7.5	2.8336	7.5	3967.514^{ce}	418.3				
3968.385	3.1234	8.5	0.0000^{o}	7.5	3968.379^{n}	508.9		0.21 ± 0.34	0.235 ± 0.001	0.240
3983.650	3.6497	7.5	0.5382^{o}	7.5	3983.659	30.4		−0.31 ± 0.34		−0.310
3988.941	5.5209^{o}	4.5	2.4136	3.5	3988.915^{ce}	47.3				
3994.512	6.1761^{o}	6.5	3.0731	7.5	3994.540^{ce}	71.3				
3996.691	3.6909	6.5	0.5896^{o}	6.5	3996.688	26.7		−0.31 ± 0.34		−0.260
4000.450	3.2011	7.5	0.1027^{o}	8.5	4000.443^{n}	321.4		0.12 ± 0.34	0.040 ± 0.002	0.040
4005.814	5.5946^{o}	7.5	2.5003	6.5	4005.839^{ce}	179.9				
4015.165	5.1227	3.5	2.0357^{o}	4.5	4015.145^{e}	23.3				
4017.748	5.4352^{o}	4.5	2.3502	3.5	4017.720^{e}	15.3				

(8) Gd I 5321.247 Å: log $gf = -1.00 \pm 0.10$ versus −0.919 (Weeks et al. 2021);

(9) Dy II 4449.704 Å: log $gf = -1.05 \pm 0.34$ versus −0.95 (Biemont & Lowe 1993);

(10) Er I 4555.697 Å: log $gf = -0.28 \pm 0.17$ versus −0.78 (Yu et al. 2019);

(11) Er II 4062.944 Å: log $gf = -1.25 \pm 0.51$ versus −1.58 (Yu et al. 2019);

(12) Tm I 4386.431 Å: log $gf = -0.93 \pm 0.25$ versus −1.07 (Wang et al. 2022);

(13) Lu I 3841.194 Å: log $gf = -0.49 \pm 0.37$ versus −0.45 (Fedchak et al. 2000);

(14) Hf II 6980.895 Å: log $gf = -2.43 \pm 0.48$ versus −1.82 (Lundqvist et al. 2006).

It appears that differences between given oscillator strengths and literature values are often better than the errors we have estimated.

5 CONCLUSIONS

In this paper, high-resolution spectroscopy of REEs turned in plasma within HC lamps is presented. Line emission spectra of neutral and singly ionized elements have been observed and wavelengths of spectral lines have been measured starting from theoretical transitions calculated from NIST energy levels data base values. Tables containing wavelength, relative intensity, and energy level classification have been compiled and, for some of the elements, estimations of the log gf have been made.

Table 22. Measured wavelengths (λ_o) and intensities of Ho I spectral lines. Meaning of symbols is given in Table 6.

λ_{Ritz} (Å)	E_{up} (eV)	J_{up}	E_{low} (eV)	J_{low}	λ_o (Å)	I (au)	Log gf Casc.	Boltz.	Nave (2003)	VALD
3774.792	3.9555^o	6.5	0.6719	5.5	3774.889^n	35525.1		−0.64 ± 0.23	−0.613 ± 0.023	
3776.076	4.3212	8.5	1.0387^o	7.5	3776.187^n	28534.1		−0.25 ± 0.23	−0.194 ± 0.021	
3783.077	4.3212	7.5	1.0448^o	7.5	3783.060^n	9340.7		−0.74 ± 0.23	−0.801 ± 0.026	
3791.543	4.4032	6.5	1.1341^o	5.5	3791.558^n	27397.5		−0.16 ± 0.23	−0.112 ± 0.022	
3792.694	4.3068	8.5	1.0387^o	9.5	3792.837^n	19756.6		−0.43 ± 0.23	−0.286 ± 0.025	
3811.928	4.2964	7.5	1.0448^o	6.5	3811.833^n	46529.7		−0.06 ± 0.23	0.045 ± 0.021	
3829.304	4.2817	7.5	1.0448^o	6.5	3829.257^n	80681.3		0.16 ± 0.23	0.159 ± 0.021	
3857.675	4.2518	8.5	1.0387^o	8.5	3857.706^n	98690.5		0.22 ± 0.23	0.410 ± 0.020	
3864.983	4.2518	7.5	1.0448^o	8.5	3864.889^n	6255.0		−0.97 ± 0.23	−0.631 ± 0.022	
3866.179	4.4137	9.5	1.2077^o	8.5	3866.196^n	4595.9		−0.90 ± 0.23	−0.670 ± 0.025	
3881.189	4.2384	7.5	1.0448^o	6.5	3881.097^n	3433.3		−1.25 ± 0.23	−1.235 ± 0.026	
3909.573	3.1704^o	7.5	0.0000	6.5	3909.560^n	39417.8		−1.58 ± 0.23	−1.774 ± 0.022	
3919.536	4.2964	6.5	1.1341^o	6.5	3919.436^n	37180.0		−0.12 ± 0.23	0.037 ± 0.022	
3951.139	4.2039^o	5.5	1.0669	6.5	3951.127^n	6526.1		−0.99 ± 0.23	−1.144 ± 0.022	
3955.829	3.1333^o	7.5	0.0000	7.5	3955.722^n	283047.7		−0.76 ± 0.23	−0.626 ± 0.021	
3967.289	4.5735	9.5	1.4493^o	9.5	3967.323^n	6467.6		−0.50 ± 0.23	−0.344 ± 0.027	
3976.916	4.3244	9.5	1.2077^o	10.5	3976.912^n	47696.3		0.04 ± 0.23	0.048 ± 0.022	
3998.229	3.7720^o	6.5	0.6719	5.5	3998.269^n	531067.6		0.37 ± 0.23	0.362 ± 0.022	
3999.509	4.3068	9.5	1.2077^o	9.5	3999.574^n	78587.3		0.24 ± 0.23	0.179 ± 0.022	
4003.353	4.1630^o	5.5	1.0669	4.5	4003.377^n	64199.2		−0.03 ± 0.23	−0.174 ± 0.022	

Table 23. Measured wavelengths (λ_o) and intensities of Ho II spectral lines. Meaning of symbols is given in Table 4.

λ_{Ritz} (Å)	E_{up} (eV)	J_{up}	E_{low} (eV)	J_{low}	λ_o (Å)	I (au)
3798.263	4.6070	5.0	1.3438^o	4.0	3798.247	1758.5
3838.383	4.5729	4.0	1.3438^o	4.0	3838.353	1045.8
3851.774	4.6070	5.0	1.3891^o	5.0	3851.803	11976.0
3896.732	3.9060	6.0	0.7253^o	6.0	3896.720	10023.5
4197.878	4.2964	5.0	1.3438^o	4.0	4197.856	675.7
4686.424	5.0005	5.0	2.3557^o	5.0	4686.394	419.8
5610.933	4.2276	6.0	2.0186^o	6.0	5610.954	1979.2
7389.357	3.6960	7.0	2.0186^o	6.0	7389.352	246.1
7465.813	4.2008	6.0	2.5406^o	7.0	7465.870	67.3
7653.765	3.6960	7.0	2.0766^o	7.0	7653.753	98.7
8545.662	3.6466	8.0	2.1962^o	9.0	8545.684	136.0
9371.477	3.5864	9.0	2.2638^o	10.0	9371.501	1600.7
9705.218	3.6466	8.0	2.3695^o	9.0	9705.253	917.0

Unlike most of the works regarding the measurement of atomic parameters, which focus on a single ion or only on certain levels of a single species, in this work a 'large-scale' systematic approach has been used with the aim of deriving maximum information from measurements. This is possible thanks to the ability of CAOS to acquire the spectrum in the whole 3700–10 000 Å range in a single exposure, ensuring the relative intensity of spectral lines during the acquisition and minimizing the necessary exposure time.

The log gf values for new observed transitions are estimated starting from lines with already known (majority from NIST-ASD) log gf values. New transition probabilities estimated with the cascade method are more reliable than those estimated with the Boltzmann method (equation 15), which should be used with caution since they rely on the hypothesis of LTE. Even if data lay on a straight line, suggesting that LTE is fulfilled for most lines, this cannot be completely true for all the transitions we observed. For this reason, log gf estimates from the Boltzmann plots should be taken as an 'order of magnitude estimate' of the quantity instead of an effective measurement. The log gf value is necessary to insert the line lists presented in this work in spectral synthesis codes, in order to identify REEs lines in stellar spectra.

In the visible range, even if a lot of studies have been already carried out, this paper adds a considerable (about 7700 new) number of holdings to existing data bases and the here reported experimental values may replace theoretical values. On the other hand, if we move to the infrared range, spectral lines data are almost completely missing. Queries to the principal data bases return no results for most of the species and very few line lists for astrophysical purposes have been compiled in the infrared, such as one by Meléndez & Barbuy (1999) that is derived by analysing the solar spectrum. The Apache Point Observatory Galactic Evolution Experiment (APOGEE) project (Majewski et al. 2017) has compiled a line list as complete as possible for the H band, which is however not published (Smith et al. 2021). A good part of these data are available in VALD. Long line lists such as those presented in this work, even if with an accuracy much worse than nowadays possible for single spectral lines emitted for example in a cooled atom trap (Dutta et al. 2016), may be a useful input for opacity calculation codes, where the

Table 24. Measured wavelengths (λ_o) and intensities of Er I spectral lines. Meaning of symbols is given in Table 6.

λ_{Ritz} (Å)	E_{up} (eV)	J_{up}	E_{low} (eV)	J_{low}	λ_o (Å)	I (au)	Casc.	Log gf Boltz.	NIST-ASD	VALD
3759.535	4.2512^{o}	7.0	0.9543	8.0	3759.536^{e}	1078.2		−0.49^{e} ± 0.17		
3761.988	4.1845^{o}	6.0	0.8898	6.0	3761.995^{e}	3208.7		−0.10^{e} ± 0.17		0.339
3768.689	4.1516	5.0	0.8627^{o}	5.0	3768.704^{e}	1031.3		−0.64^{e} ± 0.17		
3791.159	4.3382^{o}	9.0	1.0688	8.0	3791.159^{e}	1019.6		−0.38^{e} ± 0.17		0.181
3798.211	4.1261	5.0	0.8627^{o}	4.0	3798.220^{e}	1020.2		−0.67^{e} ± 0.17		−0.165
3798.628	5.2554^{o}	6.0	1.9924	6.0	3798.633^{be}	3105.9				
3798.629	3.8873	4.0	0.6243^{o}	4.0	3798.633^{be}	3105.9		−0.51^{e} ± 0.17		−0.048
3803.733	4.4179^{o}	8.0	1.1593	8.0	3803.738^{e}	414.4		−0.66^{e} ± 0.17		0.035
3815.850	5.6099^{o}	4.0	2.3616	3.0	3815.877^{be}	1830.2				
3815.880	3.2482	6.0	0.0000^{o}	5.0	3815.877^{be}	1519.2		−1.68^{e} ± 0.17		
3818.673	4.5788	4.0	1.3330^{o}	3.0	3818.695^{ce}	745.1		−0.18^{e} ± 0.17		
3825.836	3.8641	4.0	0.6243^{o}	3.0	3825.847^{e}	246.6		−1.63^{e} ± 0.17		
3827.316	3.8628	4.0	0.6243^{o}	4.0	3827.319^{ce}	1607.3		−0.82^{e} ± 0.17		−0.505
3837.126	5.5580^{o}	7.0	2.3277	7.0	3837.141^{e}	421.8		0.91^{e} ± 0.18		
3838.495	4.3884^{o}	8.0	1.1593	7.0	3838.499^{e}	2147.0		0.03^{e} ± 0.17		0.247
3839.266	4.0912	5.0	0.8627^{o}	5.0	3839.272^{ce}	3099.9		−0.22^{e} ± 0.17		
3849.915	4.2883^{o}	9.0	1.0688	9.0	3849.915^{e}	7313.9		0.43^{e} ± 0.17		0.843
3852.420	5.3683^{o}	5.0	2.1509	6.0	3852.430^{be}	1056.5				
3852.427	4.3767^{o}	8.0	1.1593	8.0	3852.430^{be}	1044.4		−0.30^{e} ± 0.17		
3854.514	4.5247^{o}	9.0	1.3090	9.0	3854.518^{e}	464.2		−0.45^{e} ± 0.17		

Table 25. Measured wavelengths (λ_o) and intensities of Er II spectral lines. Meaning of symbols is given in Table 6.

λ_{Ritz} (Å)	E_{up} (eV)	J_{up}	E_{low} (eV)	J_{low}	λ_o (Å)	I (au)	Casc.	Log gf Boltz.	Lawler et al. (2008)	VALD
3791.829	3.3235	5.5	0.0546^{o}	5.5	3791.829^{n}	1415.0		−1.05 ± 0.51	−0.922 ± 0.023	−0.920
3804.899	4.9586^{o}	8.5	1.7010	7.5	3804.930^{e}	450.7		0.68^{e} ± 0.51		
3818.712	3.8822	4.5	0.6364^{o}	3.5	3818.696^{c}	713.9		−0.58 ± 0.51		−1.204
3827.321	6.1571^{o}	8.5	2.9186	7.5	3827.319^{ce}	1607.3				
3830.482	3.2359	6.5	0.0000^{o}	6.5	3830.486^{n}	10650.3		−0.28 ± 0.51	−0.224 ± 0.022	−0.220
3832.559	4.9151	2.5	1.6810^{o}	2.5	3832.548^{e}	442.3		0.63^{e} ± 0.51		
3839.266	5.3298^{o}	5.5	2.1013	5.5	3839.272^{ce}	3099.9				0.233
3842.514	4.7879	2.5	1.5622^{o}	2.5	3842.504^{e}	208.5		0.13^{e} ± 0.51		
3849.286	3.2201	6.5	0.0000^{o}	5.5	3849.286	325.3		−1.81 ± 0.51		−1.848
3851.596	4.1046	5.5	0.8864^{o}	5.5	3851.611^{n}	311.4		−0.62 ± 0.51	−0.639 ± 0.020	−0.640
3864.317	4.7697	2.5	1.5622^{o}	1.5	3864.286^{ce}	1255.2		0.89^{e} ± 0.51		
3865.585	5.2588	4.5	2.0523^{o}	3.5	3865.563^{ce}	285.6		0.92^{e} ± 0.51		
3876.816	5.7165^{o}	6.5	2.5194	6.5	3876.795^{e}	176.5				
3880.611	3.8304	4.5	0.6364^{o}	3.5	3880.617^{n}	1736.6		−0.24 ± 0.51	−0.248 ± 0.022	−0.250
3882.886	4.0786	5.5	0.8864^{o}	4.5	3882.891^{n}	1435.5		0.02 ± 0.51	−0.146 ± 0.022	−0.150
3887.149	4.5578	4.5	1.3691^{o}	4.5	3887.165^{e}	98.1		−0.50^{e} ± 0.51		−0.640
3889.794	4.0786	4.5	0.8921^{o}	4.5	3889.799^{n}	106.6		−1.11 ± 0.51	−0.946 ± 0.022	−0.950
3890.613	4.5550	4.5	1.3691^{o}	3.5	3890.621^{e}	277.0		−0.05^{e} ± 0.51		−0.220
3895.803	4.0680	5.5	0.8864^{o}	5.5	3895.811^{n}	171.2		−0.92 ± 0.51	−0.914 ± 0.022	−0.910
3896.234	3.2359	5.5	0.0546^{o}	6.5	3896.238^{n}	13378.8		−0.16 ± 0.51	−0.118 ± 0.022	−0.120

quantity of data is usually as important (sometimes more) as their accuracy.

This work represents one step forward towards the comprehensive determination of spectral lines of REEs. It is the first of a series of works in which REE, and in general heavy elements of interest for astrophysical high-resolution spectroscopy, are spectroscopically investigated in order to measure spectral line data. Experimental data are also missing for high charge state ions for heavy elements, which are of particular interest, as pointed out above, for light curves and spectral synthesis of optical counterparts of neutron stars merging events. As it is stated in Domoto et al. (2021), since in optical counterparts of merging events (usually referred to as kilonovae) opacity in the visible and infrared ranges is dominated by atomic line absorption, the opacity calculations cannot be performed properly without taking such atomic parameters as input. Other measurements are planned in the UV and NIR ranges, and determination of line parameters for highly ionized elements has to be carried out by applying this technique to high-temperature and density plasmas. These two research path, i.e. extending measurements to other wavelength ranges and highly ionized species, have to be followed in order to achieve a comprehensive knowledge of atomic data for heavy elements.

Table 26. Measured wavelengths (λ_o) and intensities of Tm I spectral lines. Meaning of symbols is given in Table 6.

λ_{Ritz} (Å)	E_{up} (eV)	J_{up}	E_{low} (eV)	J_{low}	λ_o (Å)	I (au)	Log gf Casc.	Boltz.	NIST-ASD	VALD
3786.996	5.6275	5.5	2.3545[o]	6.5	3787.023[bce]	329.7		−0.15[e] ± 0.25		
3787.015	5.3134	8.5	2.0404[o]	7.5	3787.022[bce]	269.2		−0.59[e] ± 0.25		0.101
3798.541	4.3506[o]	2.5	1.0875	1.5	3798.542[n]	2873.8		−0.63 ± 0.25	0.027 ± 0.030	0.030
3802.080	5.1927	5.5	1.9326[o]	4.5	3802.072[n]	602.0		−0.37 ± 0.25	−0.346 ± 0.030	−0.340
3826.386	3.2393[o]	3.5	0.0000	2.5	3826.384[n]	6074.1		−1.53 ± 0.24	−1.412 ± 0.030	−1.410
3830.269	4.8627	4.5	1.6266[o]	4.5	3830.263[n]	61.5		−1.72 ± 0.25	−1.636 ± 0.078	−1.630
3840.872	5.1205	7.5	1.8934[o]	8.5	3840.868[n]	1424.8		−0.06 ± 0.25	0.206 ± 0.030	0.210
3847.515	5.3857	6.5	2.1641[o]	6.5	3847.530[e]	318.2		−0.41[e] ± 0.25		
3853.140	5.3192	3.5	2.1024[o]	2.5	3853.139[e]	116.5		−0.92[e] ± 0.25		
3872.801	5.3029	3.5	2.1024[o]	4.5	3872.818[e]	141.5		−0.85[e] ± 0.25		
3881.249	4.8202	4.5	1.6266[o]	5.5	3881.274[c]	178.0	−1.660 ± 0.029	−1.28 ± 0.25		−1.270
3883.131	3.1920[o]	3.5	0.0000	2.5	3883.126[n]	109212.9		−0.31 ± 0.24	0.158 ± 0.030	0.160
3887.347	3.1885[o]	3.5	0.0000	3.5	3887.345[n]	67359.2		−0.52 ± 0.24	−0.171 ± 0.030	−0.170
3896.617	3.1809[o]	3.5	0.0000	2.5	3896.609[n]	5404.6		−1.62 ± 0.24	−1.395 ± 0.030	−1.390
3900.804	5.2533	3.5	2.0758[o]	3.5	3900.792[ce]	166.4		−0.82[e] ± 0.25		
3913.617	4.7937	4.5	1.6266[o]	3.5	3913.630[c]	150.0		−1.38 ± 0.25		
3916.476	4.2523[o]	2.5	1.0875	3.5	3916.469[n]	26731.5		0.27 ± 0.24	0.561 ± 0.030	0.560
3917.148	5.0969	5.5	1.9326[o]	4.5	3917.144[n]	85.6		−1.28 ± 0.25	−0.875 ± 0.043	−0.880
3921.447	5.0934	5.5	1.9326[o]	5.5	3921.448[n]	96.9		−1.23 ± 0.25	−1.067 ± 0.043	−1.060
3927.354	5.3202	6.5	2.1641[o]	6.5	3927.363[e]	23.2		−1.60[e] ± 0.25		

Table 27. Measured wavelengths (λ_o) and intensities of Tm II spectral lines. Meaning of symbols is given in Table 4.

λ_{Ritz} (Å)	E_{up} (eV)	J_{up}	E_{low} (eV)	J_{low}	λ_o (Å)	I (au)
3761.914	3.2948	4.0	0.0000[o]	4.0	3761.935[b]	1210.0
3761.960	6.6221[o]	2.0	3.3274	3.0	3761.935[b]	1100.8
3778.063	5.7016[o]	5.0	2.4210	6.0	3778.065	1531.2
3786.996	7.7413[o]	3.0	4.4684	3.0	3787.023[c]	329.7
3795.759	3.2948	4.0	0.0294[o]	3.0	3795.768[b]	2172.4
3795.778	7.8364[o]	3.0	4.5711	3.0	3795.768[b]	2170.3
3832.905	6.6128[o]	5.0	3.3790	4.0	3832.877	1932.4
3848.020	3.2210	3.0	0.0000[o]	4.0	3848.023	3851.0
3861.858	6.3953[o]	4.0	3.1858	4.0	3861.874[b]	90.6
3861.881	7.5770[o]	4.0	4.3676	5.0	3861.874[b]	90.6
3881.258	7.9371[o]	3.0	4.7436	3.0	3881.273[c]	142.6
3883.440	3.2210	3.0	0.0294[o]	3.0	3883.449	354.0
3890.522	3.1858	4.0	0.0000[o]	4.0	3890.524	108.6
3900.783	4.2647	3.0	1.0873[o]	2.0	3900.792[c]	153.8
3901.995	6.6812[o]	2.0	3.5047	3.0	3902.014	343.4
3913.619	6.7470[o]	4.0	3.5800	5.0	3913.630[c]	150.0
3929.577	4.2647	3.0	1.1106[o]	3.0	3929.585	126.3
3944.155	7.2384[o]	5.0	4.0959	5.0	3944.127	100.5
3956.919	7.3971[o]	4.0	4.2647	3.0	3956.889[c]	112.4
3958.097	3.1315	3.0	0.0000[o]	4.0	3958.103	430.0

Table 28. Measured wavelengths (λ_o) and intensities of Yb I spectral lines. Meaning of symbols is given in Table 4.

λ_{Ritz} (Å)	E_{up} (eV)	J_{up}	E_{low} (eV)	J_{low}	λ_o (Å)	I (au)
3882.070	5.6365	3.0	2.4437^o	2.0	3882.070	253.4
3890.767	6.0606	2.0	2.8749^o	2.0	3890.784^c	118.0
3926.732	6.0314	3.0	2.8749^o	2.0	3926.724	68.6
3949.562	6.2070^o	1.0	3.0688	2.0	3949.587	146.0
3957.061	6.2010^o	1.0	3.0688	2.0	3957.060	61.3
3961.979	5.3591	2.0	2.2307^o	1.0	3961.981	815.4
3979.097	5.5586	1.0	2.4437^o	2.0	3979.092	267.2
3998.432	5.5436	3.0	2.4437^o	2.0	3998.432	31.7
4007.352	5.9679	2.0	2.8749^o	2.0	4007.351	11320.5
4058.405	5.9290	2.0	2.8749^o	2.0	4058.412	712.3
4063.453	5.4940	2.0	2.4437^o	2.0	4063.459	16104.0
4082.992	5.9106	3.0	2.8749^o	2.0	4082.989	3065.2
4097.906	5.8996	1.0	2.8749^o	2.0	4097.901^c	51.8
4101.334	6.0909^o	1.0	3.0688	2.0	4101.324	28.8
4121.904	6.0758^o	1.0	3.0688	2.0	4121.904	461.5
4125.535	5.8793	2.0	2.8749^o	2.0	4125.539	195.5
4134.728	6.1057	2.0	3.1080^o	1.0	4134.737^c	73.9
4163.505	6.1101^o	4.0	3.1331	3.0	4163.512	13.2
4171.214	6.0402^o	1.0	3.0688	2.0	4171.223	49.2
4172.417	6.0068^o	2.0	3.0362	1.0	4172.420	2072.3

Table 29. Measured wavelengths (λ_o) and intensities of Yb II spectral lines. Meaning of symbols is given in Table 4.

λ_{Ritz} (Å)	E_{up} (eV)	J_{up}	E_{low} (eV)	J_{low}	λ_o (Å)	I (au)
3855.881	11.4408^o	1.5	8.2263	2.5	3855.895	161.5
3890.814	9.7715	2.5	6.5859^o	2.5	3890.785^c	91.9
3892.788	8.7970	2.5	5.6130^o	3.5	3892.820	88.3
3911.290	11.1106^o	2.5	7.9417	2.5	3911.275	3964.8
3913.350	6.7327	0.5	3.5654^o	1.5	3913.357	99.9
3916.790	11.9495^o	5.5	8.7851	4.5	3916.814	69.8
4005.247	11.3209^o	3.5	8.2263	2.5	4005.237	29.7
4033.049	9.0868	5.5	6.0136^o	5.5	4033.065	115.3
4041.377	11.8639^o	3.5	8.7970	2.5	4041.344	46.1
4056.147	6.6212	2.5	3.5654^o	1.5	4056.149	267.5
4058.628	11.5013^o	3.5	8.4474	2.5	4058.633	228.0
4060.336	11.7260^o	3.5	8.6734	4.5	4060.323	203.1
4064.760	8.6300	2.5	5.5807^o	2.5	4064.783	134.3
4065.562	10.1284	3.5	7.0797^o	3.5	4065.576	35.4
4079.172	11.2648^o	2.5	8.2263	2.5	4079.169	91.6
4090.667	11.5544^o	3.5	8.5244	3.5	4090.635	32.0
4092.630	11.5273^o	3.5	8.4988	4.5	4092.637	17.9
4093.629	11.8639^o	3.5	8.8361	2.5	4093.645^b	13.6
4093.673	11.6374^o	2.5	8.6097	1.5	4093.645^b	9.9
4097.874	6.9895	2.5	3.9649^o	3.5	4097.901^c	51.8

Table 30. Measured wavelengths (λ_o) and intensities of Lu I spectral lines. Meaning of symbols is given in Table 6.

λ_{Ritz} (Å)	E_{up} (eV)	J_{up}	E_{low} (eV)	J_{low}	λ_o (Å)	I (au)	Log gf Casc.	Boltz.	NIST-ASD	VALD
4054.450	3.5699^{o}	0.5	0.5128	0.5	4054.454^{n}	3730.0		−0.78 ± 0.38	−1.004 ± 0.030	−1.000
4124.724	3.9320^{o}	1.5	0.9270	2.5	4124.715^{n}	8738.2		0.25 ± 0.38	0.134 ± 0.078	0.140
4154.094	3.9107^{o}	1.5	0.9270	1.5	4154.062^{n}	617.5		−0.93 ± 0.38	−0.760 ± 0.030	−0.760
4262.716	5.3135	2.5	2.4057^{o}	1.5	4262.725^{e}	50.3		0.48^{e} ± 0.38		
4265.976	5.3112	2.5	2.4057^{o}	3.5	4265.958^{e}	39.6		0.38^{e} ± 0.38		
4271.035	5.4124	3.5	2.5103^{o}	2.5	4271.060^{e}	152.3				
4281.018	5.4057	3.5	2.5103^{o}	4.5	4281.031^{e}	797.7				
4427.119	5.3740^{o}	0.5	2.5742	1.5	4427.107^{e}	38.0		0.52^{e} ± 0.38		
4430.455	5.2034	2.5	2.4057^{o}	3.5	4430.466^{e}	154.3		0.82^{e} ± 0.38		
4437.550	5.3674^{o}	0.5	2.5742	1.5	4437.561^{e}	19.9		0.23^{e} ± 0.38		
4464.366	5.4043^{o}	1.5	2.6279	1.5	4464.358^{e}	118.7				
4480.200	3.0138	2.5	0.2472^{o}	1.5	4480.169^{n}	326.8		−2.68 ± 0.37	−2.975 ± 0.078	−2.970
4480.200	3.0138	2.5	0.2472^{o}	1.5	4480.175	260.0	−3.074 ± 0.078	−2.78 ± 0.37		−2.970
4494.586	5.3915	4.5	2.6337^{o}	3.5	4494.566^{e}	21.4		0.32^{e} ± 0.38		
4518.556	2.7431	1.5	0.0000^{o}	1.5	4518.556^{n}	552642.2		0.09 ± 0.37	−0.558 ± 0.030	−0.560
4591.029	5.0371	1.5	2.3373^{o}	2.5	4591.054^{e}	26.1		−0.19^{e} ± 0.38		
4689.773	3.5699^{o}	1.5	0.9270	0.5	4689.773^{n}	186.0		−1.89 ± 0.38	−2.060 ± 0.078	−2.060
4716.692	2.6279	1.5	0.0000^{o}	1.5	4716.682^{n}	1684.1		−2.58 ± 0.37	−2.822 ± 0.078	−2.820
4785.385	5.3453^{o}	2.5	2.7551	1.5	4785.420^{ce}	54.2		0.72^{e} ± 0.38		
4795.927	5.4116	2.5	2.8271^{o}	3.5	4795.899^{e}	32.5		0.62^{e} ± 0.38		

Table 31. Measured wavelengths (λ_o) and intensities of Lu II spectral lines. Meaning of symbols is given in Table 4.

λ_{Ritz} (Å)	E_{up} (eV)	J_{up}	E_{low} (eV)	J_{low}	λ_o (Å)	I (au)
4785.433	4.7390^{o}	1.0	2.1489	2.0	4785.420^{c}	53.6
5476.675	4.0236^{o}	2.0	1.7604	3.0	5476.699	6087.7
6159.888	6.0420^{o}	3.0	4.0298	4.0	6159.933	45.5
6235.329	6.0176^{o}	4.0	4.0298	4.0	6235.354	19.1
6242.306	5.8153^{o}	2.0	3.8297	3.0	6242.334	32.3
7125.828	5.5691^{o}	3.0	3.8297	3.0	7125.855	7.7

Table 32. Measured wavelengths (λ_o) and intensities of Hf I spectral lines. Meaning of symbols is given in Table 6.

λ_{Ritz} (Å)	E_{up} (eV)	J_{up}	E_{low} (eV)	J_{low}	λ_o (Å)	I (au)	Log gf Casc.	Boltz.	NIST-ASD	VALD
3766.699	6.0742^{o}	2.0	2.7835	2.0	3766.725^{e}	1175.3		0.52^{e} ± 0.28		
3777.650	3.2811	2.0	0.0000^{o}	1.0	3777.664^{n}	143151.1		−0.85 ± 0.26	−0.892 ± 0.030	−0.750
3795.367	5.0687^{o}	3.0	1.8029	3.0	3795.351^{e}	474.8		−1.11^{e} ± 0.27		
3800.363	3.2615	2.0	0.0000^{o}	3.0	3800.373^{n}	78620.4		−1.13 ± 0.26	−1.363 ± 0.043	−1.080
3811.776	3.5439	3.0	0.2922^{o}	3.0	3811.785^{n}	16560.8		−1.45 ± 0.26	−1.300 ± 0.030	−1.130
3815.541	5.0383^{o}	2.0	1.7897	2.0	3815.561^{e}	321.9		−1.31^{e} ± 0.27		
3819.349	4.9925	1.0	1.7472^{o}	2.0	3819.367^{be}	342.5		−1.34^{e} ± 0.27		−0.500
3819.377	6.1525^{o}	3.0	2.9073	4.0	3819.367^{be}	305.5		0.04^{e} ± 0.28		
3820.723	3.8104	4.0	0.5663^{o}	4.0	3820.734^{n}	82934.6		−0.42 ± 0.26	−0.473 ± 0.030	−0.460
3821.216	5.8360	2.0	2.5923^{o}	3.0	3821.193^{e}	2237.5		0.52^{e} ± 0.28		
3830.013	4.9835	1.0	1.7472^{o}	2.0	3830.024^{e}	1848.5		−0.62^{e} ± 0.27		−0.050
3849.178	3.9192	2.0	0.6991^{o}	2.0	3849.190^{n}	47677.8		−0.51 ± 0.27	−0.604 ± 0.030	−0.340
3854.353	5.6696^{o}	2.0	2.4538	2.0	3854.372^{e}	268.2		−0.60^{e} ± 0.27		
3858.306	3.5047	3.0	0.2922^{o}	2.0	3858.319^{n}	44021.2		−1.06 ± 0.26	−1.049 ± 0.030	−1.060
3860.904	5.4298	5.0	2.2195^{o}	4.0	3860.921^{be}	345.3		−0.78^{e} ± 0.27		
3860.906	4.3242	2.0	1.1138^{o}	3.0	3860.921^{be}	345.3		−2.15^{e} ± 0.27		−0.840
3882.523	5.1357	3.0	1.9432^{o}	3.0	3882.534^{e}	803.9		−0.77^{e} ± 0.27		−0.080
3889.356	3.8860	2.0	0.6991^{o}	3.0	3889.367^{n}	7629.1		−1.34 ± 0.27	−1.421 ± 0.030	−1.260
3892.472	5.6381^{o}	2.0	2.4538	1.0	3892.490^{e}	149.1		−0.88^{e} ± 0.27		−0.050
3899.930	3.1782	2.0	0.0000^{o}	2.0	3899.935^{n}	118700.5		−1.02 ± 0.26	−1.320 ± 0.030	−1.140

Table 33. Measured wavelengths (λ_o) and intensities of Hf II spectral lines. Meaning of symbols is given in Table 6.

λ_{Ritz} (Å)	E_{up} (eV)	J_{up}	E_{low} (eV)	J_{low}	λ_o (Å)	I (au)	Log gf Casc.	Boltz.	Lawler et al. (2007)	VALD
3793.379	3.6458	2.5	0.3783	2.5	3793.383^{n}	11730.2		−1.18 ± 0.48	−1.110 ± 0.022	−1.110
3823.522	6.7811	2.5	3.5394^{o}	2.5	3823.525^{e}	948.6				
3849.501	5.4157	3.5	2.1958^{o}	2.5	3849.530	793.9		−0.14 ± 0.48		−0.293
3864.740	6.6917	4.5	3.4846^{o}	3.5	3864.750^{e}	165.4		0.76^{e} ± 0.49		
3877.098	6.0666	4.5	2.8697^{o}	3.5	3877.107^{e}	486.4		0.46^{e} ± 0.49		0.510
3880.817	3.6458	1.5	0.4519	2.5	3880.821^{n}	3604.8		−1.66 ± 0.48	−1.474 ± 0.028	−1.470
3882.227	6.9860	1.5	3.7933^{o}	1.5	3882.225^{e}	115.4		0.97^{e} ± 0.49		
3883.767	4.8635	2.5	1.6720	1.5	3883.769^{n}	1609.4		−0.51 ± 0.48	−1.018 ± 0.025	−1.020
3894.704	9.1333^{o}	1.5	5.9508	2.5	3894.672^{e}	279.9				
3910.877	6.5523	1.5	3.3829^{o}	0.5	3910.853^{ce}	154.7		0.57^{e} ± 0.49		
3918.094	3.6154	1.5	0.4519	0.5	3918.096^{n}	14762.7		−1.08 ± 0.48	−1.138 ± 0.022	−1.140
3923.902	4.7608	1.5	1.6020	0.5	3923.911^{n}	2609.5		−0.41 ± 0.48	−0.873 ± 0.022	−0.870
3933.190	6.5343	1.5	3.3829^{o}	2.5	3933.198^{e}	136.3		0.50^{e} ± 0.49		
3933.651	4.1877	4.5	1.0367	3.5	3933.657^{n}	719.4		−1.68 ± 0.48	−1.792 ± 0.025	−1.790
3935.632	5.3029	2.5	2.1535^{o}	1.5	3935.649	97.6		−1.16 ± 0.48		−0.911
3945.331	7.2056	2.5	4.0640^{o}	2.5	3945.347^{e}	283.4				
3964.941	5.3368	1.5	2.2107^{o}	0.5	3964.966^{c}	114.3		−1.04 ± 0.48		−0.988
3985.567	8.6148^{o}	3.5	5.5049	2.5	3985.588^{e}	116.8				
3996.006	3.4801	2.5	0.3783^{o}	1.5	3995.999^{e}	94.1	−3.342 ± 0.025	−3.41^{e} ± 0.48		
3996.796	4.7732	2.5	1.6720	3.5	3996.792^{n}	60.9		−2.00 ± 0.48	−1.581 ± 0.051	−1.580

Table 34. Measured wavelengths (λ_o) and intensities of Os I spectral lines. Meaning of symbols is given in Table 4.

λ_{Ritz} (Å)	E_{up} (eV)	J_{up}	E_{low} (eV)	J_{low}	λ_o (Å)	I (au)
3790.110	5.1111^{o}	5.0	1.8409	4.0	3790.119	1218.6
3827.141	6.0425	4.0	2.8039^{o}	4.0	3827.149	154.4
3836.064	4.3150^{o}	4.0	1.0839	4.0	3836.058	713.4
3849.978	4.8032^{o}	2.0	1.5838	2.0	3849.985	714.7
3853.442	5.4069^{o}	2.0	2.1904	1.0	3853.448	124.8
3857.086	3.7291^{o}	2.0	0.5157	3.0	3857.096^{b}	1014.5
3857.086	6.1871^{o}	3.0	2.9736	3.0	3857.096^{b}	1014.5
3876.770	4.5647^{o}	5.0	1.3676	4.0	3876.768	1414.0
3881.857	4.4533^{o}	1.0	1.2604	2.0	3881.860	971.7
3886.754	4.8032^{o}	2.0	1.6142	1.0	3886.755	97.3
3894.658	5.6488^{o}	3.0	2.4664	4.0	3894.663	114.0
3895.180	5.0693^{o}	2.0	1.8873	2.0	3895.176	143.9
3900.392	3.5175^{o}	3.0	0.3398	2.0	3900.394	800.3
3901.714	4.2606^{o}	5.0	1.0839	4.0	3901.708	217.0
3918.746	4.8199^{o}	1.0	1.6570	2.0	3918.753	37.3
3922.030	4.7440^{o}	3.0	1.5838	2.0	3922.029	26.5
3926.764	5.5630^{o}	3.0	2.4066	2.0	3926.768	75.2
3929.997	4.9952^{o}	6.0	1.8414	6.0	3929.998	144.9
3931.518	4.5633^{o}	3.0	1.4107	3.0	3931.521	92.4
3938.596	4.2309^{o}	3.0	1.0839	4.0	3938.596	2106.8

Table 35. Measured wavelengths (λ_o) and intensities of Re I spectral lines. Meaning of symbols is given in Table 4.

λ_{Ritz} (Å)	E_{up} (eV)	J_{up}	E_{low} (eV)	J_{low}	λ_o (Å)	I (au)
3895.397	5.2062^o	0.5	2.0243	1.5	3895.421	29.0
3917.266	5.2246^o	4.5	2.0605	4.5	3917.282	142.9
3929.839	4.9166^o	4.5	1.7626	3.5	3929.845	429.2
3961.033	4.8433^o	2.5	1.7142	1.5	3961.030	172.2
3962.102	6.4933^o	3.5	3.3650	3.5	3962.131	43.3
3967.396	5.8715^o	3.5	2.7474	4.5	3967.413	67.1
3981.779	7.0781^o	3.5	3.9653	3.5	3981.763	66.6
4022.959	5.6203^o	2.5	2.5393	1.5	4022.970	22.0
4028.518	5.9475^o	2.5	2.8708	2.5	4028.522	16.0
4037.491	4.9502^o	1.5	1.8803	0.5	4037.489	37.2
4061.857	4.9184^o	2.5	1.8669	3.5	4061.868	14.8
4081.427	5.0611^o	2.5	2.0243	1.5	4081.427	58.9
4089.919	4.8433^o	2.5	1.8128	2.5	4089.919	7.6
4138.534	4.9502^o	1.5	1.9552	2.5	4138.500	20.5
4146.234	5.4018^o	2.5	2.4124	2.5	4146.217	46.7
4157.252	6.5533^o	3.5	3.5719	3.5	4157.270	22.0
4159.921	6.3470^o	4.5	3.3675	4.5	4159.910	10.3
4170.387	4.6862^o	0.5	1.7142	1.5	4170.400	65.7
4188.774	6.3265^o	4.5	3.3675	4.5	4188.794	51.7
4200.472	6.5226^o	3.5	3.5719	3.5	4200.455	259.6

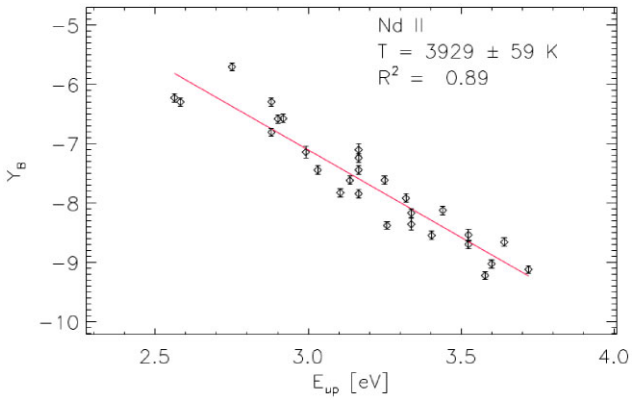

Figure 3. Boltzmann plot of Nd II spectral lines ($Y_B = \ln(\lambda I/gA)$) with here measured intensities and transition probabilities from NIST data base. The R^2 goodness-of-fit coefficient (see text for definition) is also reported.

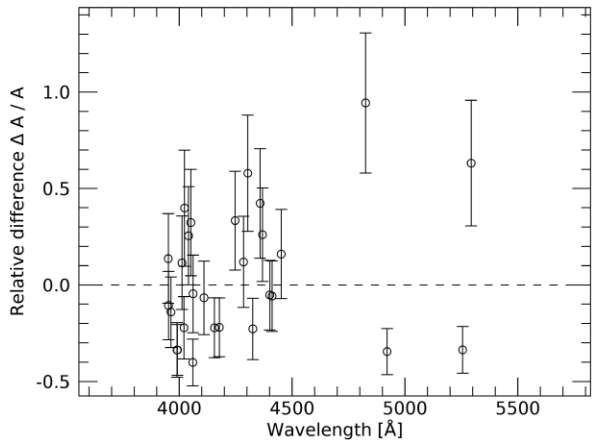

Figure 4. Relative difference $\Delta A/\langle A\rangle$ between fitted and reference A values for Nd II lines.

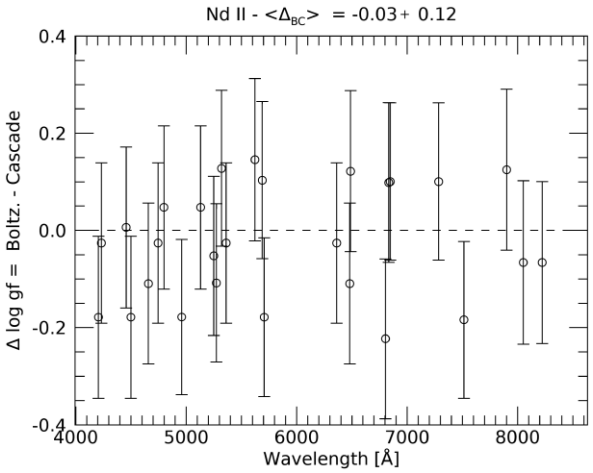

Figure 5. Comparison between Boltzmann and cascade log gf for Nd II lines.

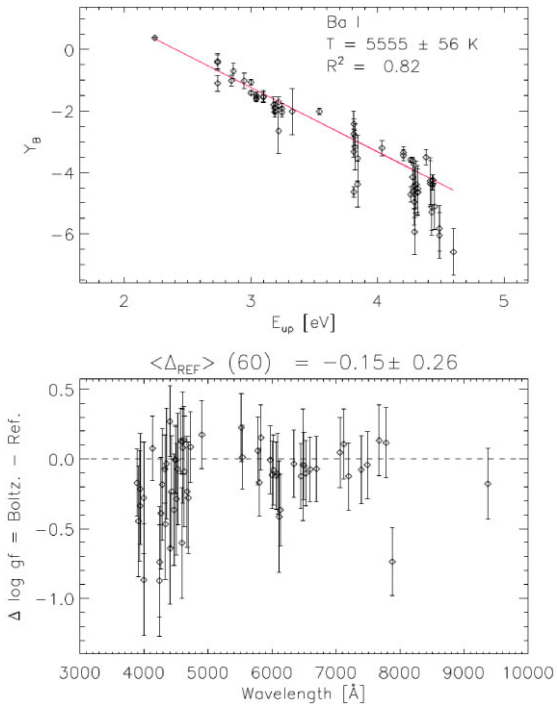

Figure 6. Top: Boltzmann plot for Ba I calibration lines ($Y_B = \ln(\lambda I/gA)$). Bottom: Ba I differences between log *gf* values and reference values for the Boltzmann method.

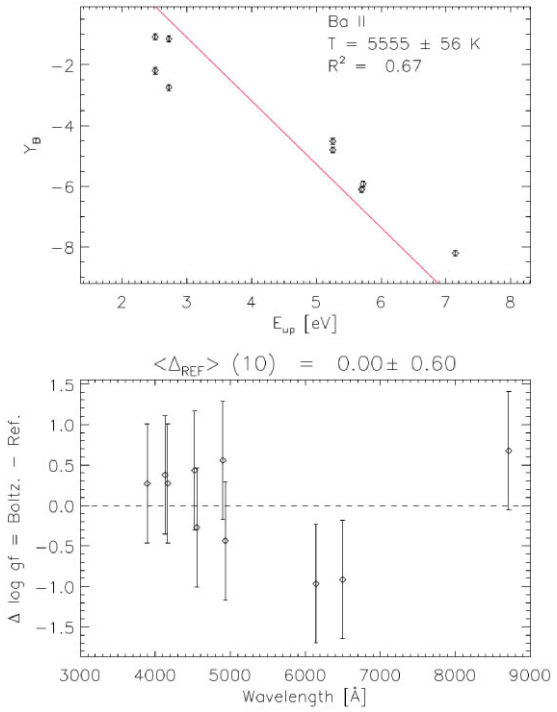

Figure 7. Same as Fig. 6 but for Ba II.

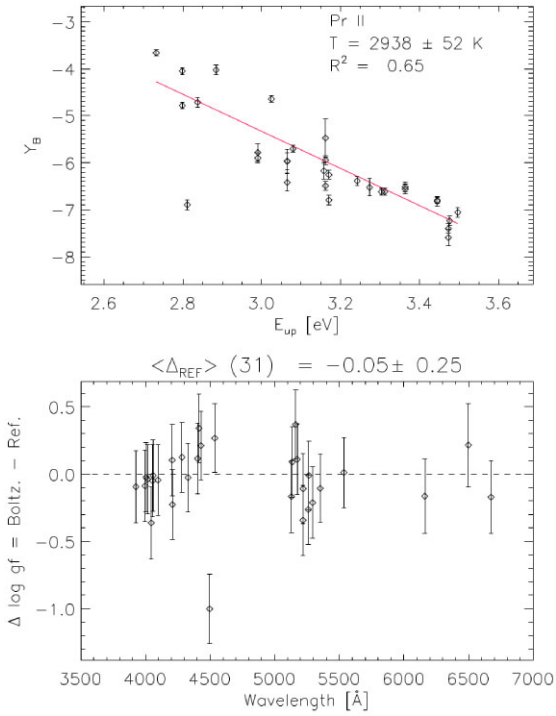

Figure 8. Same as Fig. 6 but for Pr II.

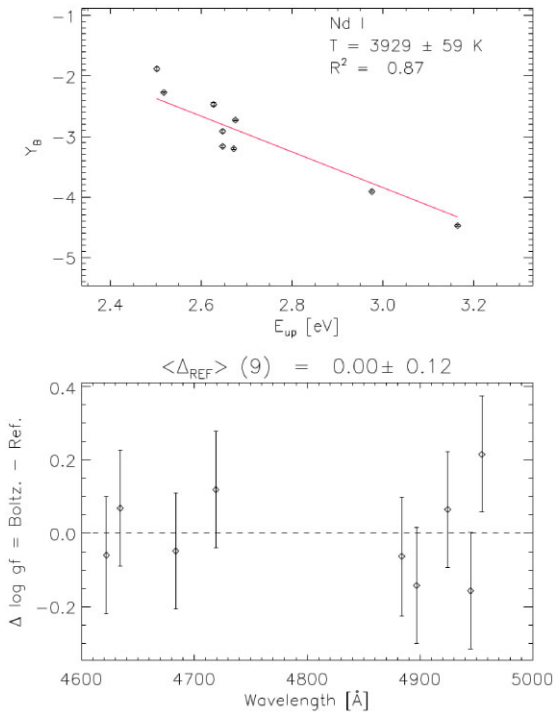

Figure 9. Same as Fig. 6 but for Nd I.

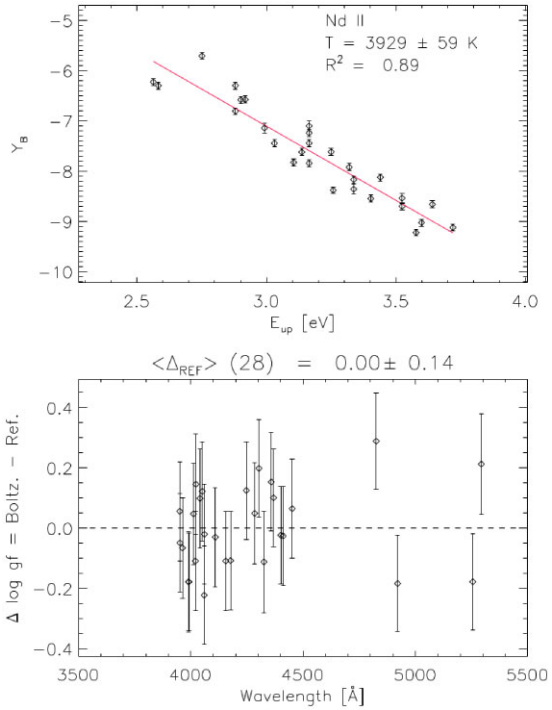

Figure 10. Same as Fig. 6 but for Nd II.

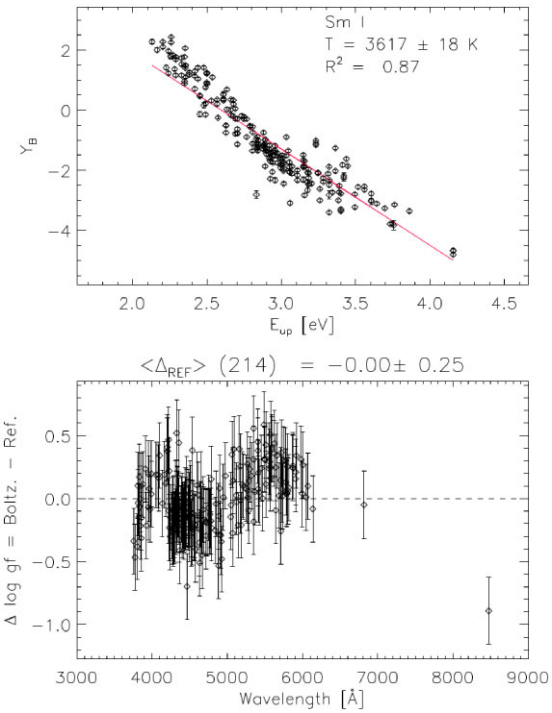

Figure 11. Same as Fig. 6 but for Sm I.

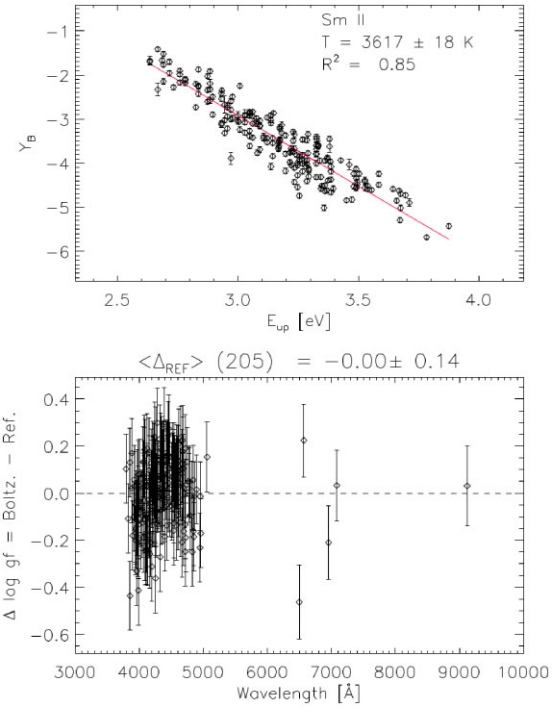

Figure 12. Same as Fig. 6 but for Sm II.

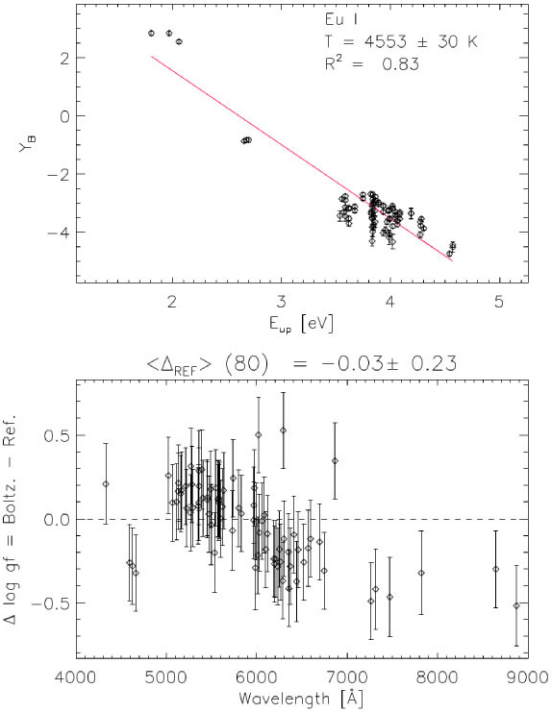

Figure 13. Same as Fig. 6 but for Eu I.

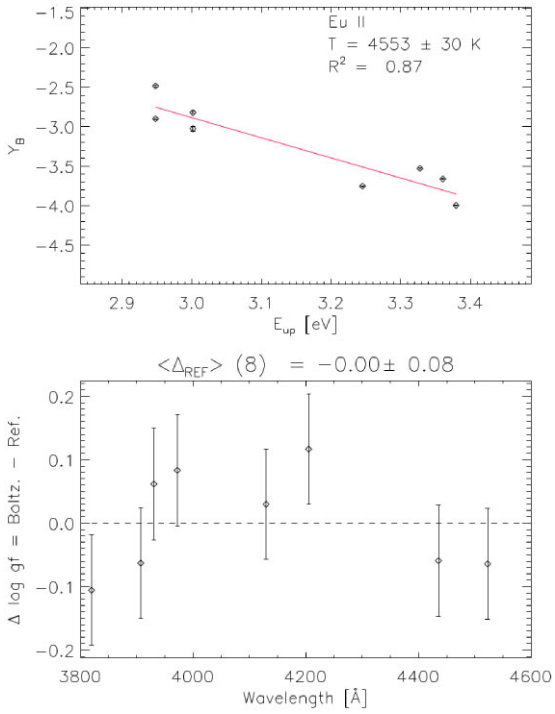

Figure 14. Same as Fig. 6 but for Eu II.

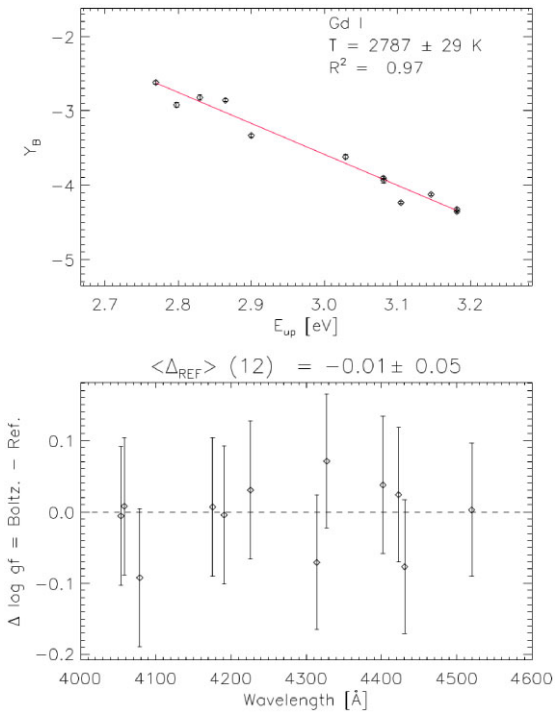

Figure 15. Same as Fig. 6 but for Gd I.

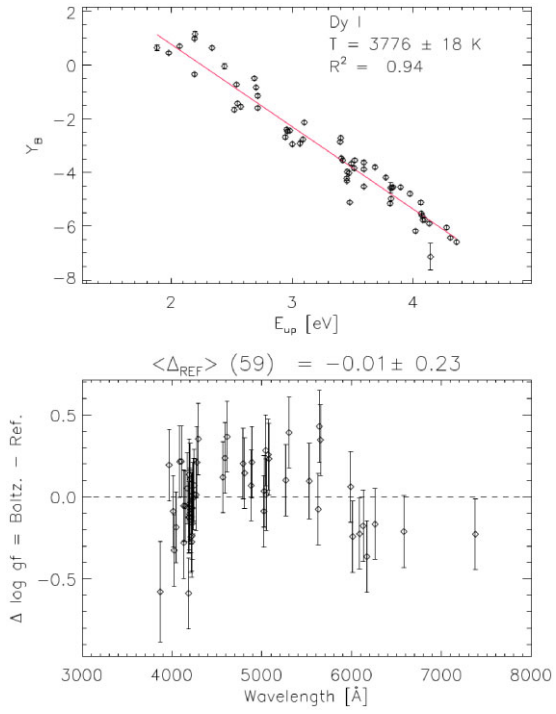

Figure 16. Same as Fig. 6 but for Dy I.

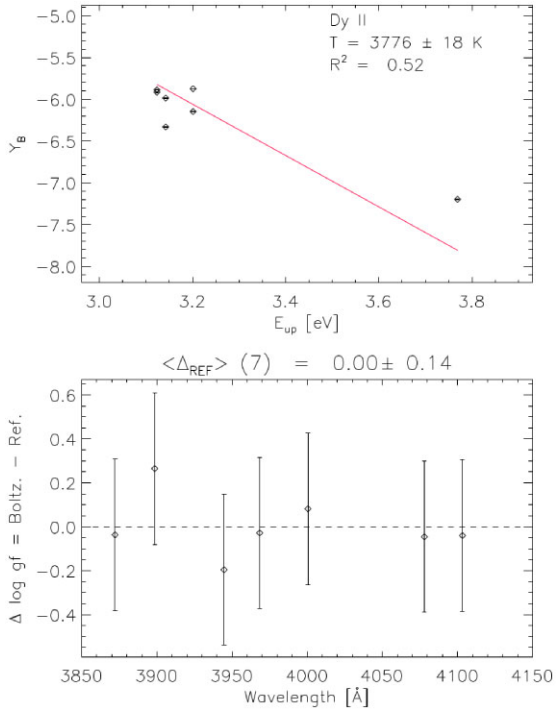

Figure 17. Same as Fig. 6 but for Dy II.

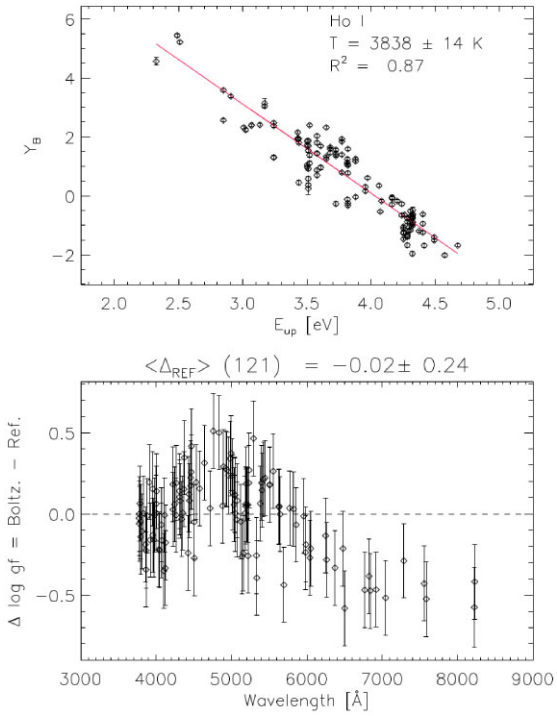

Figure 18. Same as Fig. 6 but for Ho I.

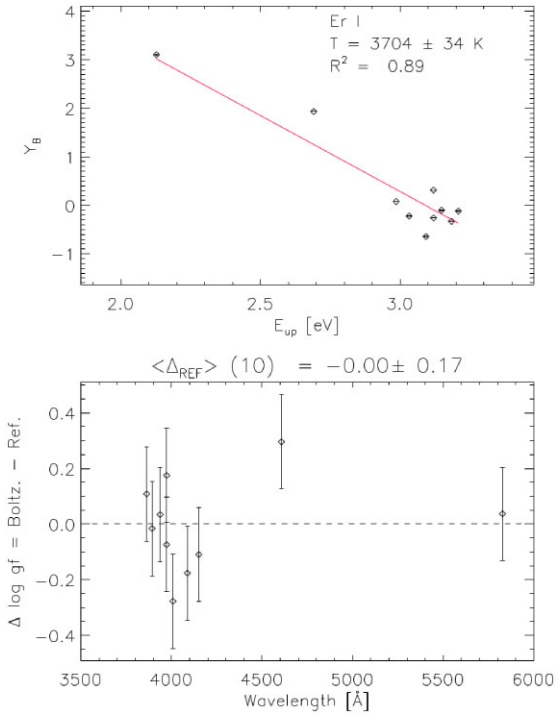

Figure 19. Same as Fig. 6 but for Er I.

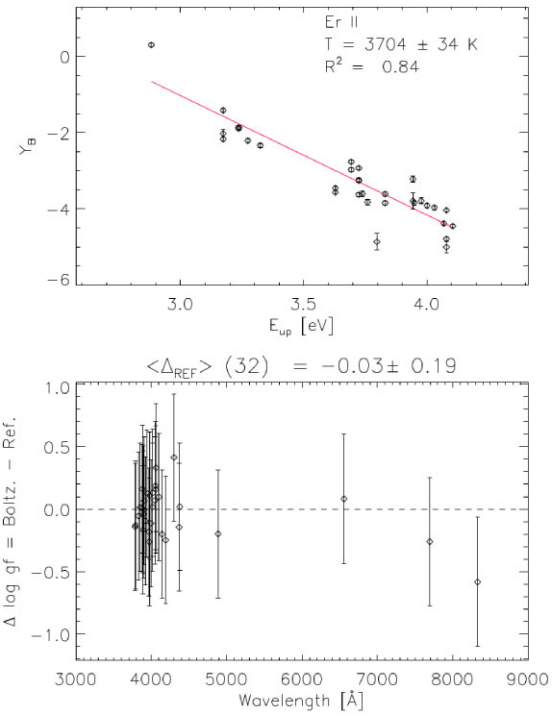

Figure 20. Same as Fig. 6 but for Er II.

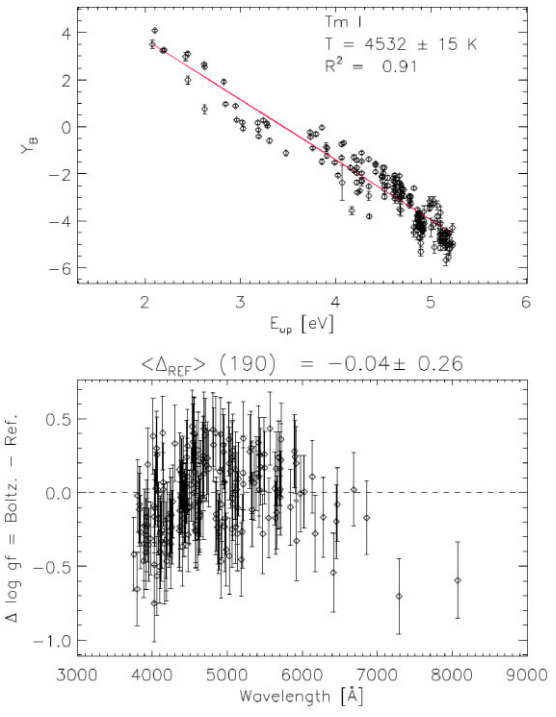

Figure 21. Same as Fig. 6 but for Tm I.

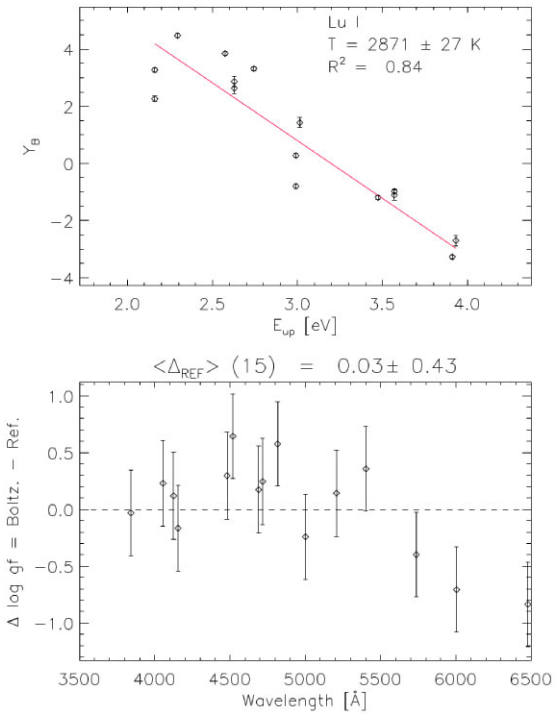

Figure 22. Same as Fig. 6 but for Lu I.

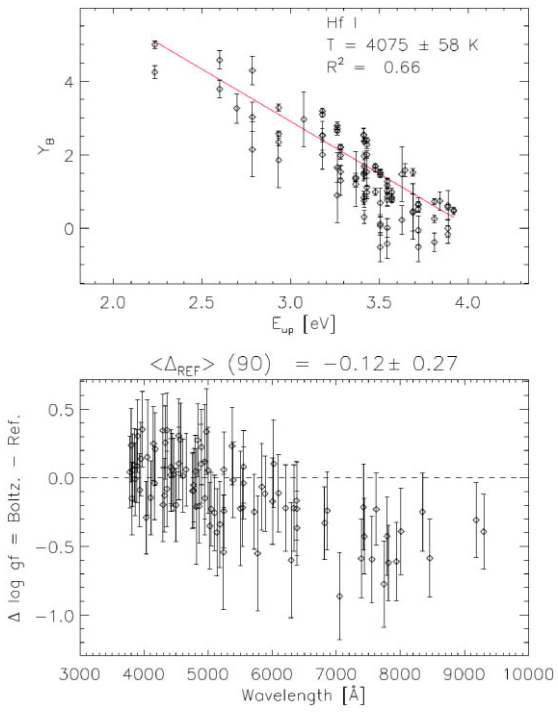

Figure 23. Same as Fig. 6 but for Hf I.

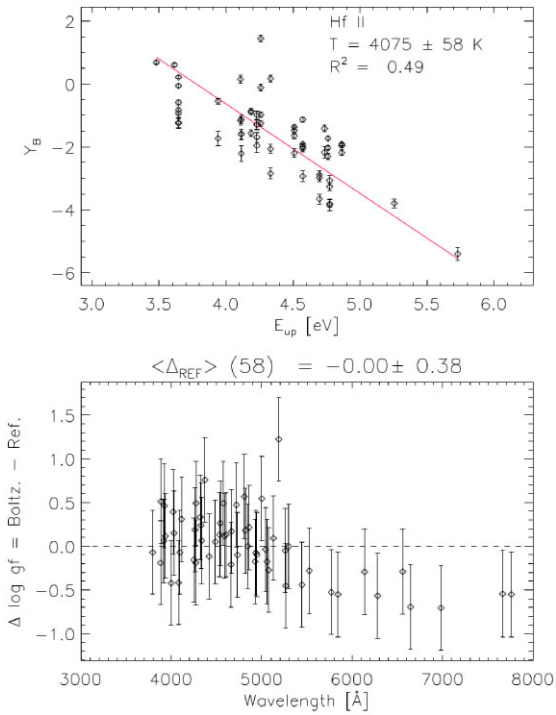

Figure 24. Same as Fig. 6 but for Hf II.

ACKNOWLEDGEMENTS

This work has made use of the VALD data base, operated at Uppsala University, the Institute of Astronomy RAS in Moscow, and the University of Vienna. Atomic data compiled in the DREAM data base (Quinet & Palmeri 2020) were extracted via VALD (Ryabchikova et al. 2015 and references therein).

DATA AVAILABILITY

The data underlying for this paper will be shared on reasonable request to the corresponding author.

REFERENCES

Biemont E., Lowe R. M., 1993, A&A, 273, 665
Cowan J. J., Sneden C., Lawler J. E., Aprahamian A., Wiescher M., Langanke K., Martínez-Pinedo G., Thielemann F.-K., 2021, Rev. Mod. Phys., 93, 015002
Domoto N., Tanaka M., Wanajo S., Kawaguchi K., 2021, ApJ, 913, 26
Dutta T., de Munshi D., Yum D., Rebhi R., Mukherjee M., 2016, Sci. Rep., 6, 29772
Fan S., Wang Q., Shang X., Tian Y., Dai Z., 2014, J. Phys. B: At. Mol. Opt. Phys., 47, 215004
Fedchak J. A., Den Hartog E. A., Lawler J. E., Palmeri P., Quinet P., Biémont E., 2000, ApJ, 542, 1109
Huber M. C. E., Sandeman R. J., 1986, Rep. Progress Phys., 49, 397
Kobayashi C. et al., 2023, ApJ, 943, L12
Kramida A., Ralchenko Y., Reader J., Team N. A., 2021, NIST Atomic Spectra Database (version 5.9), available at:https://physics.nist.gov/asd
Kramida A., Ryabtsev A. N., Young P. R., 2022, ApJS, 258, 37
Kunze H.-J., 2009, Introduction to Plasma Spectroscopy. Springer-Verlag, Berlin
Kurucz R. L., 2005, Mem. Soc. Astron. Ital. Suppl., 8, 86
Kusz J., 1992, A&AS, 92, 517

Lawler J. E., Den Hartog E. A., Sneden C., Cowan J. J., 2006, ApJS, 162, 227
Lawler J. E., den Hartog E. A., Labby Z. E., Sneden C., Cowan J. J., Ivans I. I., 2007, ApJS, 169, 120
Lawler J. E., Sneden C., Cowan J. J., Wyart J. F., Ivans I. I., Sobeck J. S., Stockett M. H., Den Hartog E. A., 2008, ApJS, 178, 71
Lawler J. E., Fittante A. J., Den Hartog E. A., 2013, J. Phys. B: At. Mol. Opt. Phys., 46, 215004
Leone F. et al., 2016, AJ, 151, 116
Lundqvist M., Nilsson H., Wahlgren G. M., Lundberg H., Xu H. L., Jang Z. K., Leckrone D. S., 2006, A&A, 450, 407
Majewski S. R. et al., 2017, AJ, 154, 94
Martin W. C., Zalubas R., Hagan L., 1978, Atomic Energy Levels – The Rare-Earth Elements. National Bureau of Standards, U.S. Department of Commerce, Washington
Meléndez J., Barbuy B., 1999, ApJS, 124, 527
Nave G., 2003, J. Opt. Soc. Am. B: Opt. Phys., 20, 2193
Nishimura N., Takiwaki T., Thielemann F.-K., 2015, ApJ, 810, 109
Quinet P., Palmeri P., 2020, Atoms, 8, 18
Ripepi V., Balona L., Catanzaro G., Marconi M., Palla F., Giarrusso M., 2015, MNRAS, 454, 2606
Ryabchikova T., Piskunov N., Kurucz R. L., Stempels H. C., Heiter U., Pakhomov Y., Barklem P. S., 2015, Phys. Scr., 90, 054005
Ryder C. A., 2011, PhD thesis, Wayne State University, Michigan
Schramm D. N., Fowler W. A., 1971, Nature, 231, 103
Smartt S. J. e. a., 2017, Nature, 551, 75
Smith V. V. et al., 2021, AJ, 161, 254
Stift M. J., Leone F., 2017, MNRAS, 465, 2880
Taylor J., 1997, Introduction to Error Analysis: The Study of Uncertainties in Physical Measurements, 2nd edn. University Science Books, New York
Tian Y., Wang X., Liu C., Yu Q., Dai Z., 2019, MNRAS, 485, 4485
Tody D., 1986, in Crawford D. L., ed., Proc. SPIE Vol. 0627, Instrumentation in Astronomy VI. SPIE, Bellingham, p. 733
Wang Q., Wang S., Kang Z., Dai Z., 2017, J. Quant. Spectrosc. Radiat. Transf., 199, 89
Wang X., Yu Q., Tian Y., Chen Z., Xie H., Zeng X., Guo G., Chang H., 2022, J. Quant. Spectrosc. Radiat. Transf., 280, 108091
Weeks R. R. D., Phillips M. C., Zhang Y., Harilal S. S., Jones R. J., 2021, Spectrochim. Acta, 181, 106199
Yu Q., Wang X., Li Q., Li Y., Dai Z., 2019, ApJS, 240, 25

SUPPORTING INFORMATION

Supplementary data are available at *MNRAS* online.

mr_tables.zip

Please note: Oxford University Press is not responsible for the content or functionality of any supporting materials supplied by the authors. Any queries (other than missing material) should be directed to the corresponding author for the article.

This paper has been typeset from a TEX/LATEX file prepared by the author.